Check for updates

View Article Online
View Journal

NJC

New Journal of Chemistry

A journal for new directions in chemistry

Accepted Manuscript

This article can be cited before page numbers have been issued, to do this please use: R. S and S. Sasidharan, *New J. Chem.*, 2020, DOI: 10.1039/D0NJ00581A.

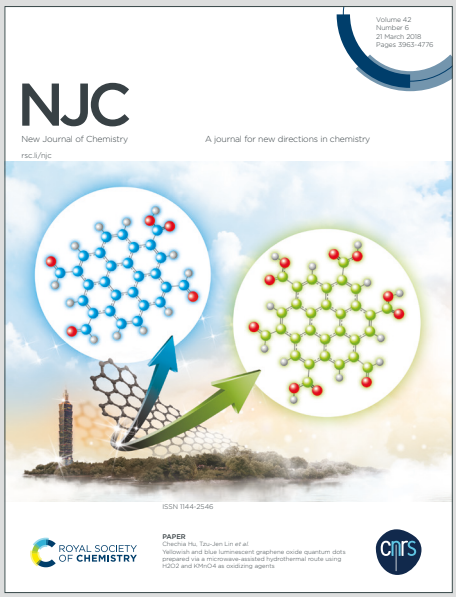

This is an Accepted Manuscript, which has been through the Royal Society of Chemistry peer review process and has been accepted for publication.

Accepted Manuscripts are published online shortly after acceptance, before technical editing, formatting and proof reading. Using this free service, authors can make their results available to the community, in citable form, before we publish the edited article. We will replace this Accepted Manuscript with the edited and formatted Advance Article as soon as it is available.

You can find more information about Accepted Manuscripts in the Information for Authors.

Please note that technical editing may introduce minor changes to the text and/or graphics, which may alter content. The journal's standard Terms & Conditions and the Ethical guidelines still apply. In no event shall the Royal Society of Chemistry be held responsible for any errors or omissions in this Accepted Manuscript or any consequences arising from the use of any information it contains.

View Article Online
DOI: 10.1039/D0NJ00581A

Transition metal mixed oxides embedded graphene oxide bilayers as an efficient electrocatalyst for optimizing hydrogen evolution reaction in alkaline media

Sarika Sasidharan[1], Rijith Sreenivasan*[1]

[1]*Post Graduate and Research Department of Chemistry, DST-FIST Supported Department, Sree Narayana College, Kollam, Affiliated to University of Kerala, Kerala-691001, India.*

* Corresponding author: rijithsreenivas@gmail.com, Phone: +919495538668

Abstract: A novel electrocatalyst containing different percentage of Iron-Titanium mixed oxide onto graphene oxide (GO) support was prepared by embedding via thermal decomposition method (TD) and coated it on Cu substrate through facile electroless Ni-Co-P plating. Explore the GO embedding for improving the catalytic properties of composites towards the electrocatalytic hydrogen evolution reactions (HER) in alkaline media. The optimized mixed oxide embedded GO exhibit superior electrocatalytic activity related to favourable surface structure and electrochemical properties, which has been further confirmed by X-ray diffraction (XRD), HRTEM, SEM-EDS, XPS analysis and electrochemical analysis. It is found that a benchmark current density of 6.02 mA/cm^2 has been achieved at an overpotential of 104 mVdec^{-1} in 1 M KOH with lower Tafel slope of 37 mVdec^{-1}. The prepared catalyst was economically viable and performance was consistent over a wide span of time. The remarkable activity of FTG incorporated electrode can be ascribed to the synergetic effect of Ti, Ni and Phosphorous elements over the reactive sites and also due to the increased electrical conductivity. The binder free coating of active ingredients over working electrode surface also enriches the catalytic behaviour. These findings may open a new insights on design and construction of novel, efficient and durable electrocatalysts for HERs.

Key words: Graphene oxide; mixed oxide electrocatalyst; Ni-Co-P; HER; Electrochemical analysis

Published on 10 July 2020. Downloaded by Karolinska Institutet University Library on 7/10/2020 4:06:52 PM.

New Journal of Chemistry Accepted Manuscript

View Article Online
DOI: 10.1039/D0NJ00581A

Published on 10 July 2020. Downloaded by Karolinska Institutet University Library on 7/10/2020 4:06:52 PM.

1. Introduction

Modern society has an urge for futuristic renewable and environmentally benign energy sources. Hydrogen can be alternative to carbon fuel economy which satisfies all the criteria for an efficient energy source. Even though water electrolysis provides high purity hydrogen production, via conventional routes faces many crises like extremely high cost and low yield. The electrode materials practically used in alkaline water electrolysis are not only costly, but also less effective due to the slow and sluggish hydrogen evolution reaction (HERs) kinetics due to the consumption of H^+ ions derived from water dissociation (Volmer step) instead the direct usage of hydronium ions from the electrolytes [1, 2] in alkaline media. So numerous efforts were employed for its sustainable production from various electrolytic methods. An earth abundant - robust electrocatalyst with nearly low overpotential, high selectivity, stability and activity are indispensible for HER. The platinum electrocatalyst has an excellent catalytic activity towards HER, which offers an over potential close to zero, with Tafel slope around 30 $mVdec^{-1}$ corresponds to a large current density [3-5], but its application is limited due to high cost and low abundance in nature. The utilization of non-precious metal catalyst for making advanced electrochemical appliance render safe, clean and durable hydrogen dependent energy system, so researchers are focused more on transition metal electrocatalyst with noble metal electronic configuration for HERs.

TiO_2 is extensively used as a most promising electrocatalyst due to its strong oxidising power, high chemical stability, inexpensive, nontoxic, sustainable and reliable performance. The catalytic activity, physical characteristic and reaction kinetics of TiO_2 can be improved by introducing transition metal dopant having partially filled d orbitals into its frame work which leads to more diverse functionalities. Literature reviews shows that transition metal oxide such as Co_3O_4, MoO_2, MnO_2 and V_2O_5 incorporated TiO_2 has an enhanced catalytic activity, chemical stability, diffusion barrier properties and morphological character than bare TiO_2. Thus mixed oxide catalyst surface modifies the hydrogen binding energy, as well as weaken the O-H bond of adsorb water over the catalyst surface through enhanced exchange current density over monometallic oxide / alloy catalyst. The incorporation of Fe_2O_3 on TiO_2 has wide application in catalysis [6], catalytic oxidation [7], electrochemical water splitting [8] and chlorine evolution [9]. But overpotential for the HER is still higher than precious metals, which attributed to a low exchange current density and further slowdown the transport kinetics in the HER process, mainly originates from low active surface area and poor electrical conductivity of electrocatalyst. Therefore, a new novel

New Journal of Chemistry Accepted Manuscript

View Article Online
DOI: 10.1039/D0NJ00581A

strategy can be envisaged to design mixed metal oxide materials on efficient support material like graphene oxide which yields selective water dissociation by offering a large surface area, high thermal and electrical conductivity and stability to wide pH conditions. In mixed metal oxide incorporated graphene oxide (GO), the metal nanoparticles act as a sphere to enhance the distance between the GO sheets and lead to increase in the surface area of heterogeneous catalyst system.

In the light of many reports, heterogeneous mixed oxide electrocatalyst was one of the promising HER active electrocatalyst, the catalytic activity of mixed oxide composite can be reinforced by the incorporation of it in Ni-P matrix. The catalytic activity of bare nickel coatings has improved by mixing it with transition metal through their synergic effect and which further resist the intermittent electrolytic rate over the substrate surface [10-11]. The cobalt incorporated ternary alloy of Ni-P has found to be more active toward HER than binary alloy of Ni. The metal composite coating on Ni-Co-P ternary matrix serves as an efficient HER electrocatalyst. The composite incorporated on alloy nanoparticles leads to good conductivity and facilitates electron transport [12]. Thus an electrocatalyst with an improved catalytic activity is developed by exploring the benefits of electroless alloy - composite coating and specific surface area of nanocomposite of mixed oxide. Henceforth we report herein the synthesis and application of a novel Fe-Ti mixed oxide embedded GO onto Cu substrate by electroless Ni-Co-P ternary alloy coating method and its morphological, structural and electrochemical performance as an efficient cathode material for HER.

2. Experimental Section

2.1. Preparation of GO and GO embedded catalysts

GO was synthesized from expandable graphite that procured from Sigma Aldrich via modified Hummers method [13]. The synthesis route of GO was depicted in **Scheme.1.(i).** TD method was opted for the preparation of Fe_2O_3-TiO_2-GO mixed oxide composite. The materials used were anhydrous ferric chloride, titanium isopropoxide and graphene oxide procured from Sigma Aldrich. The required amount of 1:1 metal-metal molar ratio of $Ti(O\text{-}iPr)_4$ and $FeCl_3$ are dissolved in definite concentration of isopropanol and magnetically stir the solution for 5 h at room temperature in order to homogenize the solution. Then evaporated to dryness in a china dish followed by heating at 120 ^{0}C for 1 h in an air oven. The resulting powder of Fe_2O_3-TiO_2 (FT composite) was then ground using a mortar and pestle and calcined at 450 ^{0}C for 1 h in a controlled muffle furnace for the complete conversion of

Published on 10 July 2020. Downloaded by Karolinska Institutet University Library on 7/10/2020 4:06:52 PM.

New Journal of Chemistry Accepted Manuscript

View Article Online
DOI: 10.1039/D0NJ00581A

$FeCl_3$ and $Ti(ipr)_4$ into its corresponding oxides. For the preparation of GO - supported mixed oxide composite (here after it is designated as FTG), 50 mg finely powdered GO was added to the 1:1 homogeneous solution containing FT and stirred for 2 h.

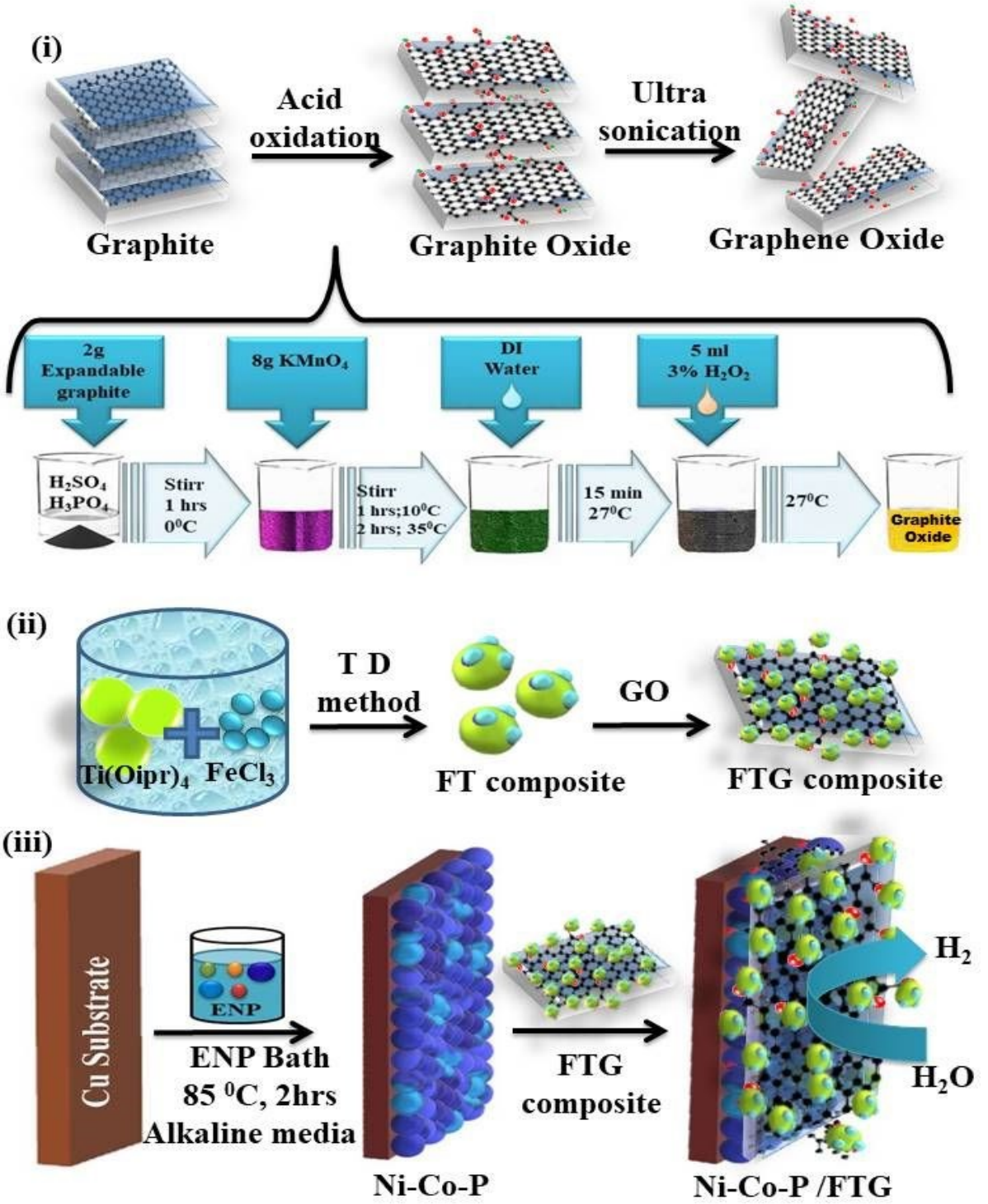

Scheme.1. Schematic representation of the preparation routes of GO, FTG composite and FTG composite coated electrode.

Published on 10 July 2020. Downloaded by Karolinska Institutet University Library on 7/10/2020 4:06:52 PM.

New Journal of Chemistry Accepted Manuscript

View Article Online
DOI: 10.1039/D0NJ00581A

Evaporate the whole solution to dryness in a china dish, subsequently heat it in an air oven at 120 ^{0}C for 3 h for the deposition of FT onto GO. The resulting composite was grounded using a pestle and mortar and again heated at 500 ^{0}C on muffle furnace to obtain FTG mixed oxide catalyst.

2.2. Development of FTG incorporated Ni-Co-P coatings

The FTG reinforced Ni-Co-P ternary matrix was developed by electroless alloy-composite plating method. The substrate used for the present study was high purity copper sheets (99.8 %, MTI Corporation) having dimension 1 cm × 1 cm × 0.25 cm and these were polished using 600, 1500 and 2000 emery paper and cleaned by trichloroethylene to avoid grease and other adhered impurities from the surface of the substrate**.** Finally washed with ultrapure water to decontaminate the surface. After physical and chemical treatment of the substrate, it undergoes a two-step activation process. In first step, cleaned and mechanically polished substrate surface was treated with a solution of $SnCl_2$/HCl and then it was placed in a nucleation bath having $PdCl_2$/HCl. After the surface activation process, the pre-treated substrate was further used to create electrochemical coatings of FTG by electroless plating process. For plating, the nickel bath was mixed with surfactants, reducing agents, complexing agent and mixed oxide catalyst for the effective coating on the substrate. A commonly accepted autocatalytic deposition of EN plating [14, 15] is as follows:

$$H_2PO_2^- + H_2O \rightarrow H^+ + HPO_3^{2-} + 2H_{ad} \quad (1)$$

$$Ni^{2+} + 2H_{ad} \rightarrow Ni + 2H^+ \quad (2)$$

$$H_2PO_2^- + H_{ad} \rightarrow H_2O + OH^- + P \quad (3)$$

$$H_2PO_2^- + H_2O \rightarrow \quad H^+ + HPO_3^{2-} + H_2 \quad (4)$$

The electroless plating process was repeated by varying different amount of prepared composites in the bath and the prepared electrodes were represented as Ni-Co-P/FTG1, Ni-Co-P/FTG2, Ni-Co-P/FTG3 and Ni-Co-P/FTG5 corresponds to the FTG concentration 1 g/L, 2 g/L, 3 g/L and 5 g/L, respectively in the bath. In addition to this Ni-Co-P plate without composite and pure Ni-P bath were prepared for further comparative study of electrodes. The composition of the plating solution and the operating conditions has great influence on the properties of the substrate. The factors like pH, temperature and concentration of bath components will also affect the coating process. The pH of the plating bath was maintained at

Published on 10 July 2020. Downloaded by Karolinska Institutet University Library on 7/10/2020 4:06:52 PM.

New Journal of Chemistry Accepted Manuscript

View Article Online
DOI: 10.1039/D0NJ00581A

8.0 by adding ammonia solution. The main advantage of these baths includes low cost and greater ease of process control. The composition of plating bath and conditions as given in **Table 1.**

Table 1. Electroless bath composition

Sl. No	Chemicals used	Bath composition g/L
1	Nickel sulphate	10
2	Cobalt sulphate	10
3	Trisodium citrate	15
4	Sodium hypophosphate	20
5	Ammonium sulphate	15
6	Composite	1 – 5
Temperature: 80 ± 2 °C; pH :8; Duration : 2 hours		

2.3. Characterization of Catalyst and Coatings

The morphology, particle size and composition of catalysts and coatings were analysed by using field emission scanning electron microscopy JEOL JSM – 840A coupled with energy dispersive X-ray (EDX unit). The HRTEM images and SAED patterns at different magnifications were obtained from JEOL JEL 2100 E-Japan. The crystalline structure of the prepared catalyst and catalyst coated plates were evaluated by using X-ray diffractometer using Cu-Kα radiation (λ = 1.542 A°) with a 2θ ranging from 10 to 80 ° (X'Pert Pro) at a scan rate of 0.035 °/ sec with a tube voltage of 40 kV and a tube current of 30 mA. The Fourier Transform - Infrared analysis (Perkin-Elmer spectrum 2) was performed over the range of 4000- 400 cm^{-1} to investigate the structural and functional groups present in the catalyst. An idea about the band gap of catalyst was carried out in a spectral range of 200-800 nm using UV spectrometer (Schimadzu UV-2450 analyzer) and Tauc plot from Kubelka-Munk transformation. The phase structure and elemental composition analysis of FTG was done by X-ray photo electron spectroscopy (XPS) using AXIS Ultra DLD Kratos Analytical Ltd. U K.

Published on 10 July 2020. Downloaded by Karolinska Institutet University Library on 7/10/2020 4:06:52 PM.

New Journal of Chemistry Accepted Manuscript

View Article Online
DOI: 10.1039/D0NJ00581A

Published on 10 July 2020. Downloaded by Karolinska Institutet University Library on 7/10/2020 4:06:52 PM.

2.4. Physical Characterization of Coatings

The porosity of the prepared FTG reinforced Ni-Co-P coatings were analysed by ferroxyl reagent test. The test reagent contains a solution of potassium ferricyanide, sodium chloride and agar-agar in hot water. The FTG incorporated plate after the immersion to test reagent in 15 m develops deep prussian blue colourized pits which can be visualised directly to measure the porosity of coatings. Adhesion characteristics of electroless coatings were carried out using scratch test method. The procedure for the test is the rapid removal of an adhesion tape firmly fixed onto the coated plate having 10 parallel cuts placed 1mm space apart. The coating adhesion was ranging from 0 to 5 according to the international standards ISO2409 [GB/T]. The thickness of coating was calculated by the equation;

$$T = \frac{\Delta W}{(A - \rho)} \quad (5)$$

; Where T is the thickness of the coating, ΔW is the coating weight (difference in weight of the substrate before and after coating), ρ is the coating density and A is the area of coating. Vicker's micro hardness indenter – Shimadzu HMV-2000 was used for the analysis of micro hardness of the coatings. It was calculated by considering the mean value of 5 measurements taken at different location on the top of coating surface on applying a load of 100 g for 10 s duration.

2.5. Electrochemical characterizations

The HER activity of the catalyst were evaluated using a three electrode system. The catalyst modified electrodes were act as working electrode, a saturated calomel electrode (SCE) as the reference electrode and a graphite rod as counter electrode for electrochemical measurements and was investigated using an electrochemical work station Biologic Potentiostat-SP200. The CV, CA, LSV, EIS and polarization studies of coating were tested in 1.0 M NaOH solution. The potentiodynamic linear polarization studies of the FTG modified plates were carried out at a scan rate of 20 mV/s in potential range between -0.2 V to + 0.2 V. The Tafel parameters such as overpotential, η (V), exchange current density, i (Acm^{-2}) and Tafel slope, b ($Vdec^{-1}$) were calculated by Tafel fitting using the software EC Lab V 10.40 and Tafel equation [16].

$$\eta = a + b \log i \quad (6)$$

New Journal of Chemistry Accepted Manuscript

View Article Online
DOI: 10.1039/D0NJ00581A

$$a = \frac{2.303\ RT}{\alpha nF} \log(i_0) \quad (7)$$

$$b = -\frac{2.303\ RT}{\alpha nF} \quad (8)$$

The electrochemical impedance analysis was carried out in a frequency ranging from 100 KHz to 10 MHz by frequency respond analyser. The electrochemical experimental data fitting and analysis was performed using EC Lab V 10.40 software.

3. Results and Discussion

3.1. Phase analysis and stability of composite

The crystal phase characteristics and crystalline purity of prepared composites were evaluated using XRD analysis. **Fig.1.** The XRD pattern of prepared GO was compared with the graphite. A sharp well-defined peak at 2θ = 11.68° corresponds to (001) plane in XRD pattern of GO, which is in good agreement with previous studies [17] and an absence of peak around 2θ = 26.58° indicates the successful conversion of raw graphite powder to GO. Due to the lack chemical reactivity of graphite, some surface defects were introduced to make it easier for modification by incorporating oxygen containing functional groups such as epoxy, carbonyl, hydroxyl to synthesis of GO. Using Scherer equation it was found that GO has a high interlayer distance as compared to graphite which reveals the attachment of chemical groups and thus indicates the conversion of graphite to GO. The grain size of the composite was evaluated using the equation.

$$D = \frac{K\lambda}{\beta Cos\theta} \quad (9)$$

Where D, K, λ, β and θ are crystalline size, Debye coefficient, wave length, FWHM and Bragg's angle respectively. The average size of composite was found to be 179 nm.

The XRD pattern of FTG composite shows the coexistence of rutile TiO_2 and pseudo brookite Fe_2TiO_5 phase. A well-defined sharp peak at 2θ value 27.79°, 41.87°, 54.32° for (211), (221) and (501) planes, respectively corresponds to the rutile TiO_2 (JCPDS file no: 21-1276) and pseudobrookite was confirmed by the peaks at 36.05°, 56.37° and 62.90° corresponds to (411), (104) and (032) planes, respectively (JCPDS file no: 41-1432). The incorporation of GO on to FT was confirmed by the peak at 2θ = 11.68°.

Published on 10 July 2020. Downloaded by Karolinska Institutet University Library on 7/10/2020 4:06:52 PM.

New Journal of Chemistry Accepted Manuscript

View Article Online
DOI: 10.1039/D0NJ00581A

As a result of thermal treatment, the guest metal oxides react with titania to form new crystalline phases. During the reaction Fe-Ti solid solution (Fe_xTiO_Y) was formed [18 -19] due to the migration of metallic cations along with dehydroxylation reaction. Pseudo brookite along with rutile crystalline phase coexist with anatase was produced as per the reaction

$$TiO_2(2Fe^{3+}) + 3O^{2-} \longrightarrow Fe_2TiO_5 \qquad (10)$$

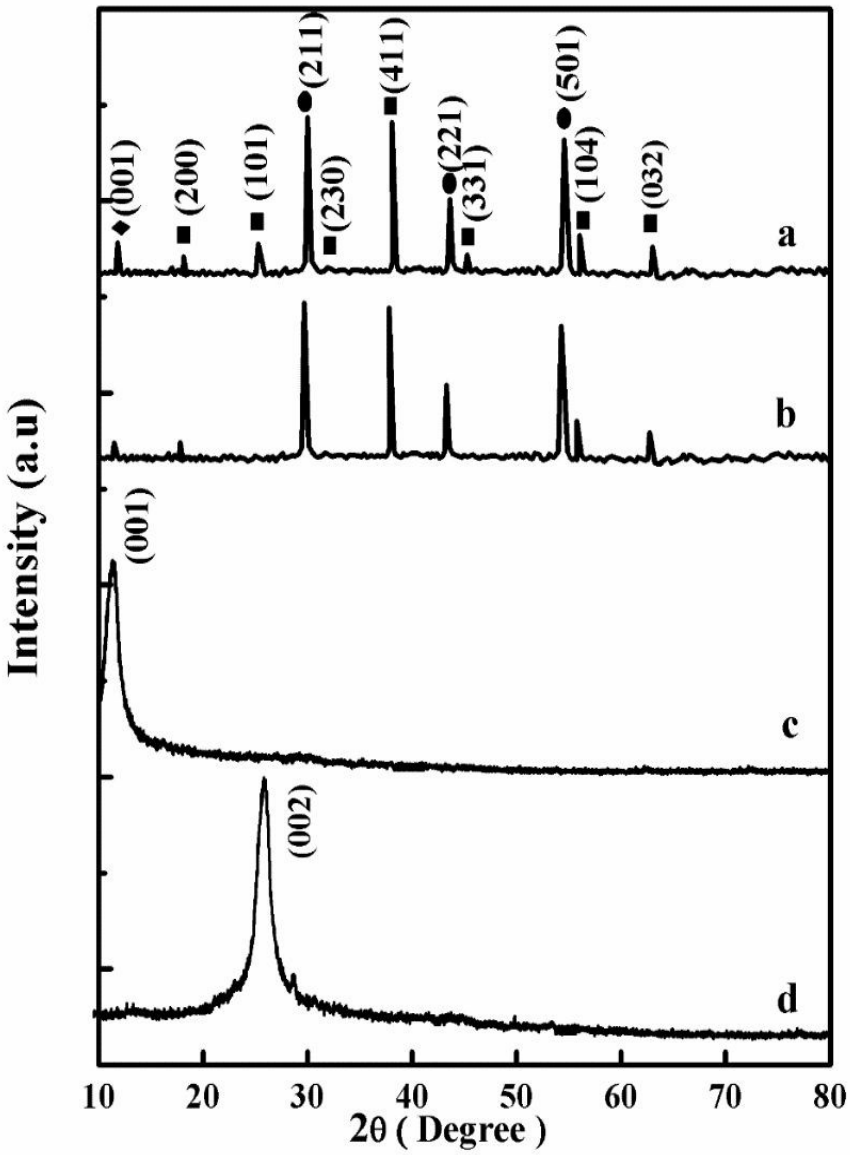

Fig.1. XRD pattern of (a) FTG (b) FTG obtained from electroless bath (c) Graphene oxide (d) Expandable Graphite.

In the Fe:Ti (1:1) sample, initially anatase and brookite phase were formed (< 200 °C) and then it converted to pseudobrookite (< 400 °C) and after that, it will be rutile phase [20]. As a result of phase transformation the crystalline size of the phases was also increased, while

Published on 10 July 2020. Downloaded by Karolinska Institutet University Library on 7/10/2020 4:06:52 PM.

New Journal of Chemistry Accepted Manuscript

View Article Online
DOI: 10.1039/D0NJ00581A

the composite heated over 500 °C the Fe_2O_3 (haematite) was formed which separated from Fe-Ti-O solid solution thereby decrease the surface area of composite. A remarkable change seen in solid state reaction and crystalline phase transfer with calcination temperature. The Fe content and calcination temperature crucially influence the Ti defect concentration in crystal lattice. The Fe ratio in Fe:Ti was optimized for maximum Ti crystal defect concentration and the calcination temperature was fixed within 500 °C, the XRD results clearly illustrates the crystal properties of new phases and the HRTEM images also agree with the results. Lower the Fe:Ti ratio favours the formation of Fe_2TiO_5 phase [21]. Furthermore, all the diffraction peak were sharp and narrowed, which indicates the significance of high degree of crystallinity, which also agree with the results of HRTEM images.

The physical and chemical stability of composite were characterized by comparative analysis of peak intensities, number and 2θ values in the XRD pattern of composite filtered from EN bath with pure composite. It was found that the peak intensities, numbers and 2θ values are almost equal for both the composite, which reveals the enhanced crystallinity with lack of crystal defects enrich the FTG composite to exhibit higher rate of HER activity.

3.2. UV-Visible and FTIR spectral analysis

The electronic environment around GO, TiO_2, Fe_2O_3, FT and FTG were studied by using UV-Visible analysis and FTIR analysis, it was illustrated in **Fig.2.A** and **Fig.2.B**, respectively. The amount of Fe content in the sample was identified from the UV spectra in which the absorption edge was broadened and the peak was centred between a wavelengths of 460 - 520 nm. The presence of pseudobrookite Fe_2TiO_5 phase was confirmed by an absorption peak observed at 590 nm having a band gap of 2.17 eV reported in literature [21]. The formation of Fe_2TiO_5 can be explained by the accumulation of Fe rich layers at the surface of TiO_2 at elevated temperature [22]. The characterization of this iron layer over the rutile phase was further confirmed by HRTEM analysis. The pure crystalline TiO_2 has a band gap 3.1 eV corresponds to the absorption onset peak around 400 nm due to the electronic transition from 2p of Oxygen to 3d of Ti, which confirms it is in rutile rather than anatase phase. The incorporation of Fe_2O_3 and GO to TiO_2 cause an absorption shift to higher wave length region, which occur by the substitution of Ti^{4+} in TiO_2 matrix by Fe^{3+} resulting in the formation of a solid solution of Fe_2TiO_5 entrapped in GO. Also an absorption band around 520 nm developed due to the presence of Fe rich TiO_2 surfaces in FTG composite.

Published on 10 July 2020. Downloaded by Karolinska Institutet University Library on 7/10/2020 4:06:52 PM.

New Journal of Chemistry Accepted Manuscript

View Article Online
DOI: 10.1039/D0NJ00581A

Published on 10 July 2020. Downloaded by Karolinska Institutet University Library on 7/10/2020 4:06:52 PM.

The FTIR spectra of the prepared composite and its precursors were recorded in the range 400 cm^{-1} – 4000 cm^{-1} depicted in **Fig.2.B.** The band at 550 cm^{-1} and 466 cm^{-1} associated with the vibration of Fe-O stretching [23]. The peak centred at 594 cm^{-1} is due to Ti-O stretching in TiO_2. The band at 1363 cm^{-1} and 1233 cm^{-1} in GO were due to the stretching vibration of tertiary C-OH group and epoxy group, respectively. The peaks at 1586 cm^{-1} and 1063 cm^{-1} were ascribed the aromatic stretching vibration and C-O stretching vibrations, respectively. The existence of C=O and C–O, confirmed the oxidization of graphite to GO and was consistent with the peaks reported in the earlier research works [24]. The main structure of graphite layer was still retained after modification. The prepared FTG composite with IR spectral peaks centred at 3208 cm^{-1} (OH), 1616 cm^{-1} (aromatic C=C), 1918 cm^{-1} (carbonyl C=O), 1158 cm^{-1} (Ti-OH), 1063 cm^{-} (^{1}epoxy C-O), 590 cm^{-1} (Ti-O) and 529 cm^{-1} (Fe-O). The peaks between 500 and 630 cm^{-1} was attributed due to the metal oxide- metal oxide interactions in the composite. The result of spectral analysis confirms the successful synthesis of composite and identification of chemical interactions of the moieties associated with the precursor materials.

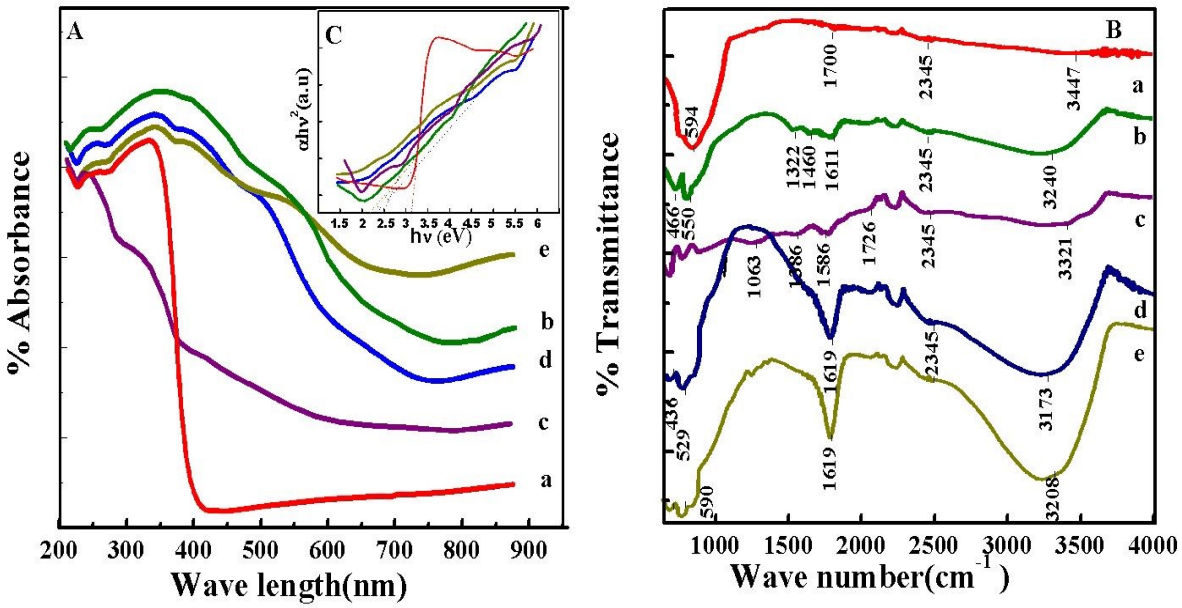

Fig.2. (A) UV-Visible spectra of (a) TiO_2 (b) Fe_2O_3 (c) GO (d) FT and (e) FTG and inset **(C)** Tauc plots. **(B)** IR spectra of (a) TiO_2 (b) Fe_2O_3 (c) GO (d) FT and (e) FTG

3.3. Surface Morphology Analysis

The HRTEM image of GO and prepared composites were studied and depicted in **Fig.3.** GO was found to have a wavy wrinkled sheet nature. A high transparency in TEM

New Journal of Chemistry Accepted Manuscript

View Article Online
DOI: 10.1039/D0NJ00581A

image of GO reveals that it possess lack of multi-layers of GO sheets. In the SAED patterns rings with sharp spots in GO indicates the polycrystalline nature having hexagonal six fold symmetry [25] and the multiple spots were due to the domain overlapping and back-folding of edges.

Almost all of the particles in the composite were enriched with other species present in the composite such that as pair wise combination of each particles over different material on GO surface and can be clearly visible from TEM images. This was evidenced by the XRD studies suggesting the formation of pseudobrookite, Fe_2TiO_5 phase by the enrichment of a layer of Fe^{3+} on the surface of TiO_2 forming a solid solution phase [22] and were entrapped in GO sheet. The ring shaped SAED pattern also suggests the polycrystalline mixed oxide nature of FTG rather than coupled oxide. From SAED pattern the fringe width 7.09 [1/nm] and the corresponding d spacing 0.28 nm were obtained for FTG composite.

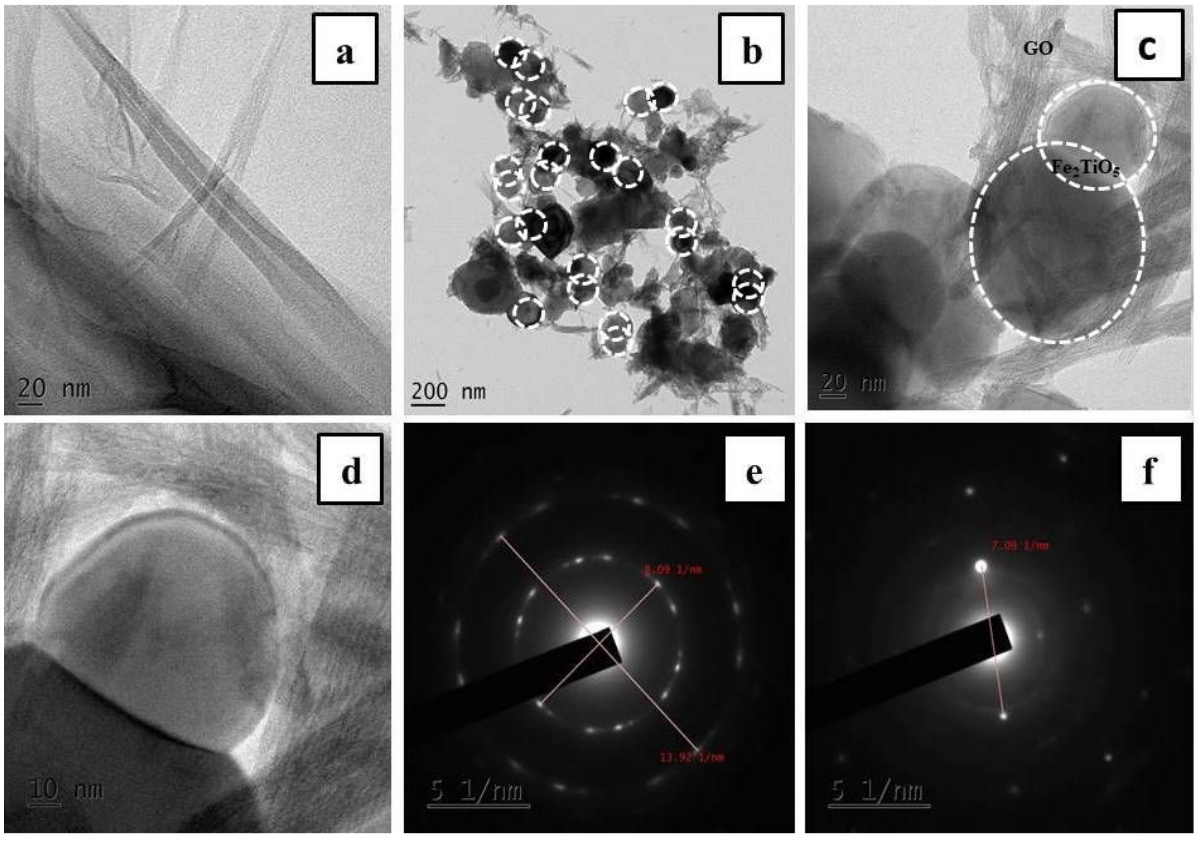

Fig.3. TEM images of (a) GO (b) FTG (c)-(d) different magnification of FTG composite and (e) SAED pattern of GO and (f) SAED pattern of FTG composite

Published on 10 July 2020. Downloaded by Karolinska Institutet University Library on 7/10/2020 4:06:52 PM.

New Journal of Chemistry Accepted Manuscript

View Article Online
DOI: 10.1039/D0NJ00581A

Published on 10 July 2020. Downloaded by Kalinska Institute University Library on 7/10/2020 4:06:52 PM.

3.4. XPS analysis

XPS analysis was carried out inorder to study the chemical compositions and forms of titania and iron cations present in FTG composite. The XPS spectra were depicted in **Fig.4.** In the XPS survey scan of FTG mixed oxide composite the presence of elements such as Titanium, Iron, Carbon, and Oxygen were identified . The existence of Fe^{3+} in the surface was detected by the bands centred at 711.18 eV and 725.50 eV corresponds to $2P^{3/2}$ and $2P^{1/2}$, respectively [26]. In Ti 2P spectrum, the peak located at 458.91 eV and 464.69 eV were due to the spin-orbit splitting of Ti^{4+} to Ti $2P^{3/2}$ and Ti $2P^{1/2}$, respectively [27]. The XPS spectra of C 1s contains three peaks located at 284.50 eV for C-C (sp^2 carbon), 286.14 eV for O-C-O/O-H and 288.43 eV corresponds to C=O, respectively [28]. In the deconvoluted spectrum of O 1s contains two peaks at 529.94 eV and 531.5 eV corresponds to the oxygen from quinone groups and carbonyl groups, respectively.

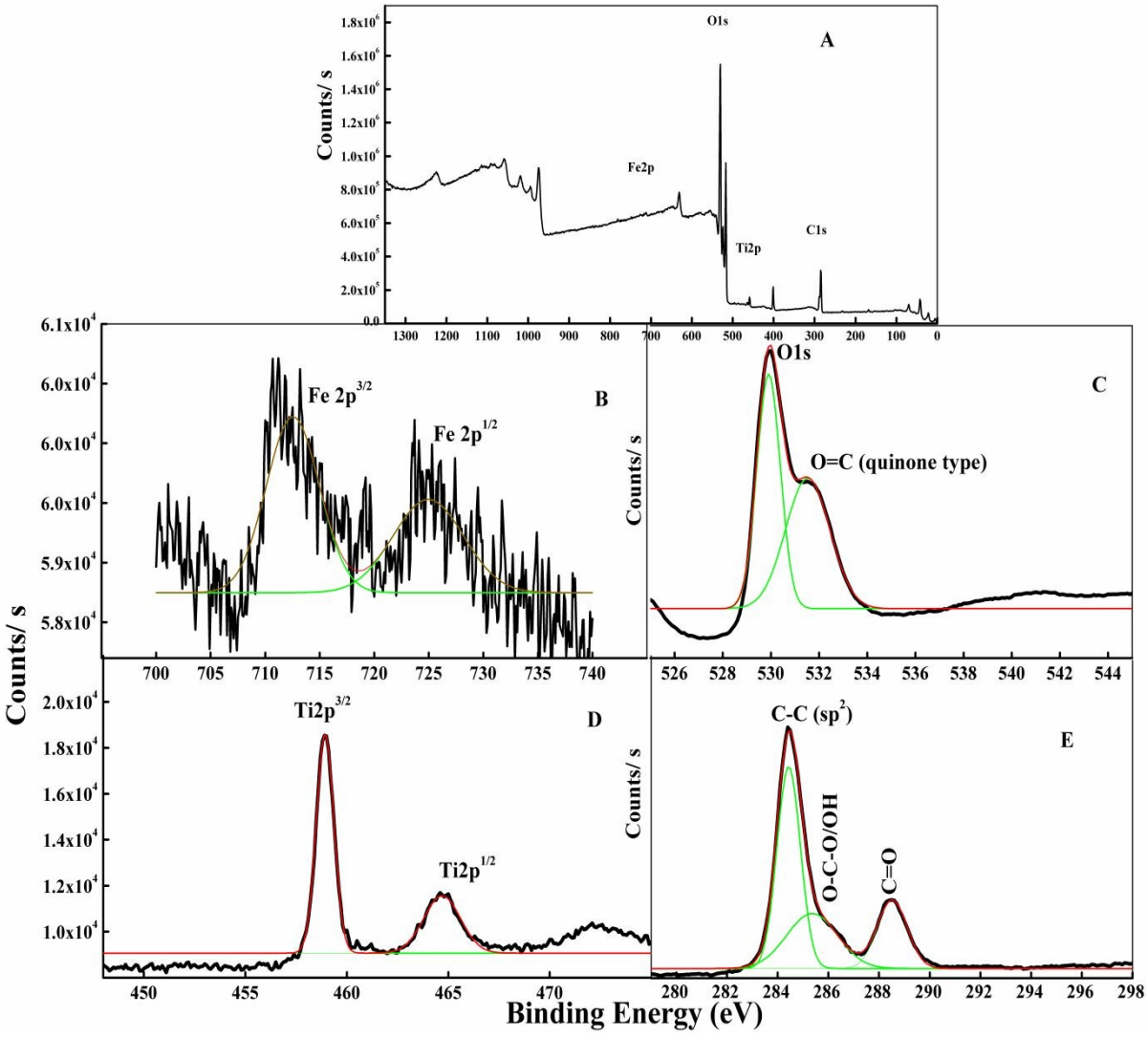

Fig.4. XPS spectra of (A) FTG (B) Fe2p (C) O1s (D) Ti2p (E) C1s

New Journal of Chemistry Accepted Manuscript

Published on 10 July 2020. Downloaded by Karolinska Institutet University Library on 7/10/2020 4:06:52 PM.

3.5. Morphological and Compositional Analysis of Coatings

View Article Online
DOI: 10.1039/D0NJ00581A

The SEM image of various electroless nickel coatings were depicted in **Fig.5.** The improved morphology of FTG incorporated Ni-Co-P as compared to bare Ni-Co-P ternary coating and bare Ni-P binary alloy coating was clearly visible from the SEM images. Pure Ni-P shows smooth uniform granular nodules whereas Co incorporation results in a non-uniform distribution of nodules on the surface. The appearance of cauliflower like nodules was observed in earlier structure for electroless Ni-P coating [29]. The composite incorporation further creates non- uniform distribution provides a higher surface area resulting in enhanced catalytic activity towards HER. The incorporation of Co into Ni-P matrix was confirmed by the SEM analysis which is also in good agreement with the EDX analysis. An optimized Ni-Co-P/FTG3 shows a homogeneous distribution of FTG composite over Co incorporated Ni-P matrix which leads to an increased compactness of coating as well as enhanced surface area and high catalytic activity.

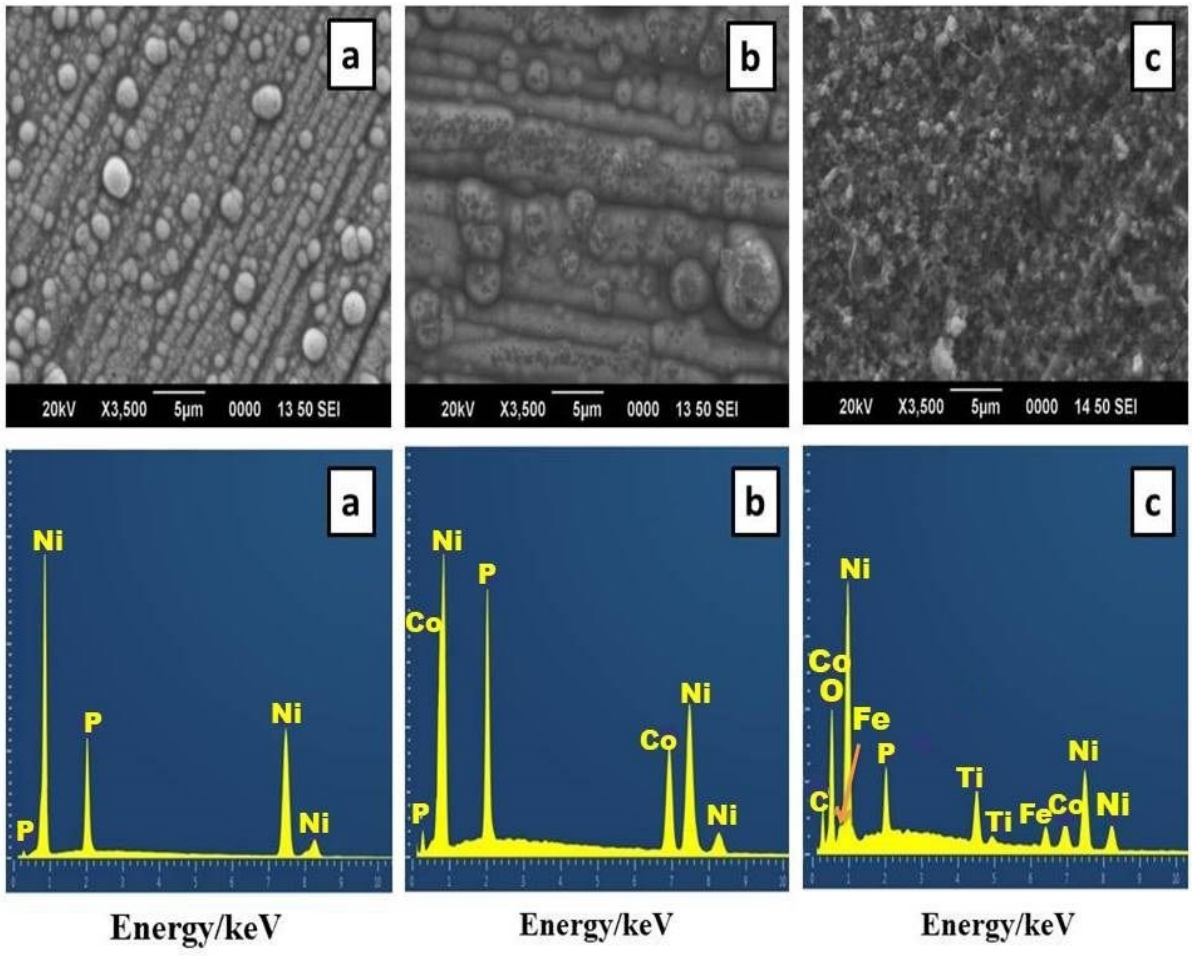

Fig.5. SEM images and EDS spectrum of (a) Pure Ni-P coating (b) Ni-Co-P ternary coating (c) Ni-Co-P/FTG3, respectively.

New Journal of Chemistry Accepted Manuscript

View Article Online
DOI: 10.1039/D0NJ00581A

The EDS data (**Table 2)**, elemental distribution and wt % of all the elements over the surface of Ni-P, Ni-Co-P and FTG3 incorporated plates were taken for the surface analysis. The phosphorus content has a leading role in determining the microstructure of electroless Ni-P coatings. Previous research reports states that the electroless Ni-P possess microstructures such as γ form (amorphous), β form (crystalline) and γ-β form (both form coexist) based on a low, high and medium phosphorous content, respectively in the coating [30]. An electroless plate with phosphorus content less than 9 wt. % deforms the crystallinity [31] and considered to possess amorphous phase and was confirmed by the well-defined cauliflower like nodular structures seen in SEM image [32]. The SEM image along with EDX data shows that the composite incorporation did not affect the microstructure nature of coating which is in good agreement with literature [33]. The EDS mapping was carried out for studying the distribution of various elements in the electroless plate and that of Ni-Co-P/FTG3 was shown in **Fig.6.**

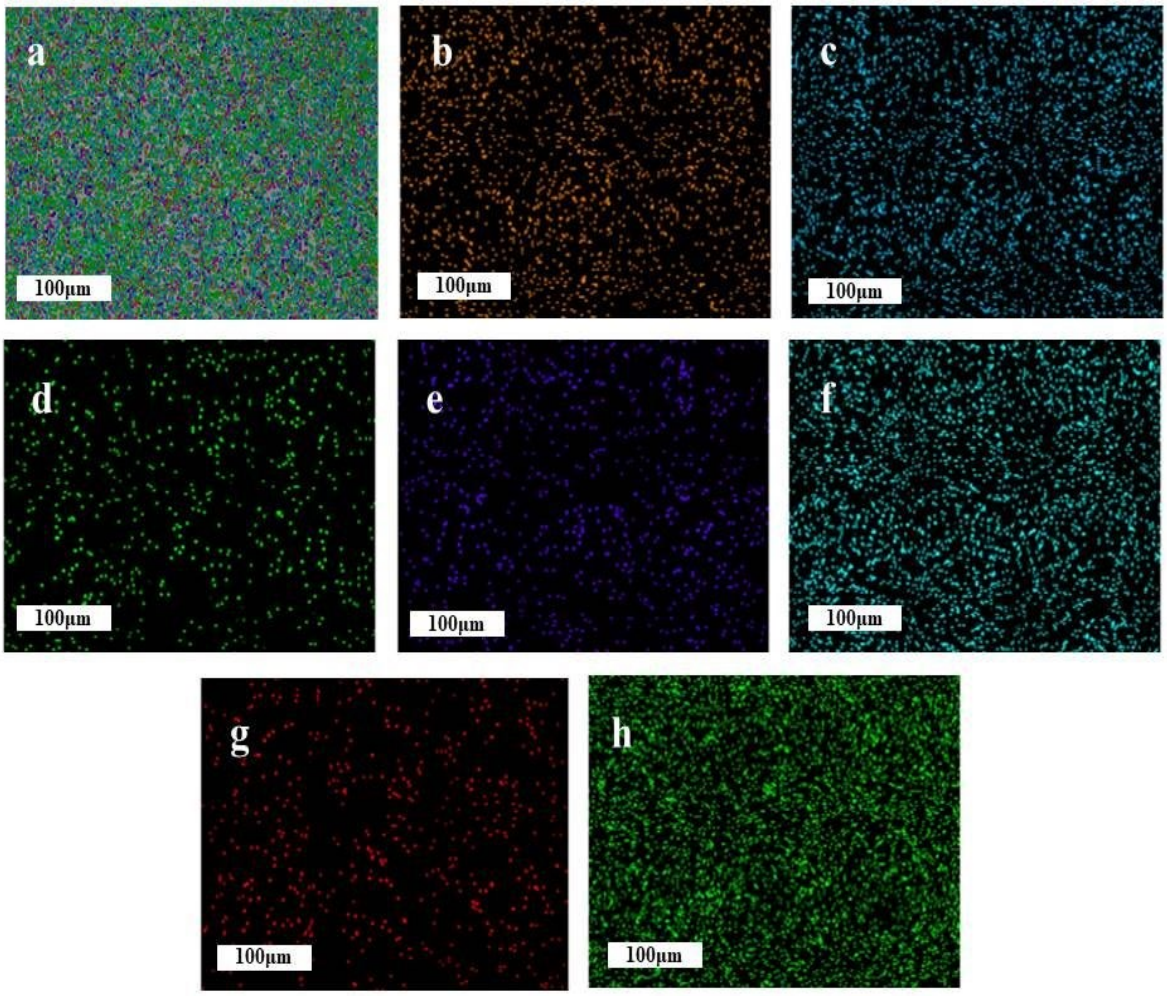

Fig.6. EDS mapping of (a) optimized Ni-Co-P/FTG3 plate, Ni-Co-P/FTG3 with the distribution of Oxygen (b) Cobalt (c) Iron (d) Carbon (e) Phosphorous (f) Titanium (g) and Nickel (h)

Published on 10 July 2020. Downloaded by Karolinska Institutet University Library on 7/10/2020 4:06:52 PM.

New Journal of Chemistry Accepted Manuscript

View Article Online
DOI: 10.1039/D0NJ00581A

EDS data authenticate the uniform distribution of Ni, Co, P, Fe, Ti and C over the plate. Since the FTG3 incorporated plate contains a high phosphorus content of 13.24 %, it prevents the nucleation of fcc Ni and thus evidence for the amorphous phase of Ni-P matrix.

Table 2. EDS analysis of electroless coatings

Coatings	**Ni** (Wt %)	**P** (Wt %)	**Co** (Wt %)	**C** (Wt %)	**Ti** (Wt %)	**Fe** (Wt %)	**O** (Wt %)
Pure Ni-P	88.50	11.50	-	-	-	-	-
Ni-Co-P	61.18	14.77	24.03	-	-	-	-
Ni-Co-P/FTG3	59.11	13.24	10.28	5.66	2.44	1.72	7.40

3.6. Physicochemical Characterization of Coating

Mainly the hardness of electroless coatings depends on phosphorus (P) content, temperature and plating duration. The hardness of coating decreases by the increasing level of P content, due to the presence of a large number of amorphous phase microstructures. The hardness of coating was estimated by VHT test. Also the electroless Ni-P composite coatings are harder than pure electroless Ni-P coating [34]. Fe_2O_3 and TiO_2 were reported to be hard oxides thus it enhanced the hardness of composite coatings. This can be also explained by dispersion strengthening effect [35]. More over the Co incorporation has a vital role in enhancing the microhardness of electroless nanocomposite coating [36]. The VHN value for pure Ni-P, Ni-Co-P and composite incorporated Ni-Co-P plates were 429, 542 and 642, respectively. From this observation the hardness of the coating was successively increases and reaches a maximum at the composite incorporation to Ni-Co-P. The thickness of Ni-Co-P/FTG3 (16.4 μm) was found to be greater than Ni-Co-P (14.3 μm) and Ni-P (12 μm) coating. The porosity and amorphous nature of the composite incorporated Ni-Co-P was verified by the prussian blue colouration obtained during the ferroxyl reagent test. The adhesive nature of composite onto the Ni-Co-P plate was higher than the pure Ni-P and Ni-Co-P plate, it was verified by standard scratch test procedure.

3.7. X-Ray diffraction studies of Coatings

The XRD pattern of electroless coatings were shown in **Fig.7.** The crystallinity of composite coatings was confirmed by the XRD analysis. The XRD patterns of all the coatings shows a common peak of 2θ values at 44.5° and 52.3° corresponding to (111) and (200) plane

Published on 10 July 2020. Downloaded by Karolinska Institutet University Library on 7/10/2020 4:06:52 PM.

New Journal of Chemistry Accepted Manuscript

View Article Online
DOI: 10.1039/D0NJ00581A

of Nickel incorporated onto the surface of substrate [37]. The grain size of Ni particles were calculated by Debye-Scherrer equation and it was found to be 1.2 nm. The diffraction pattern of Ni-Co-P shows a sharp peak at 2θ value of 74.5° which indicates the effective incorporation of cobalt onto the Ni-P matrix [37-38], which also increases the d spacing of nickel in Ni-P [39]. The addition of FTG onto Ni-Co-P plate was less significantly contributed to the crystalline phase shift of pure Ni-Co-P matrix and the results resembles the study of Balaraju et al [40]. The distribution of Ti and Fe over the surface was not predominant and the peak appeared at 27.80° and 36.05°, which illustrate the presence of Ti as TiO_2 corresponds to plane (211) and Fe in Fe_2TiO_5 with (411) plane over the substrate surface. These results are correlated well with the EDX results.

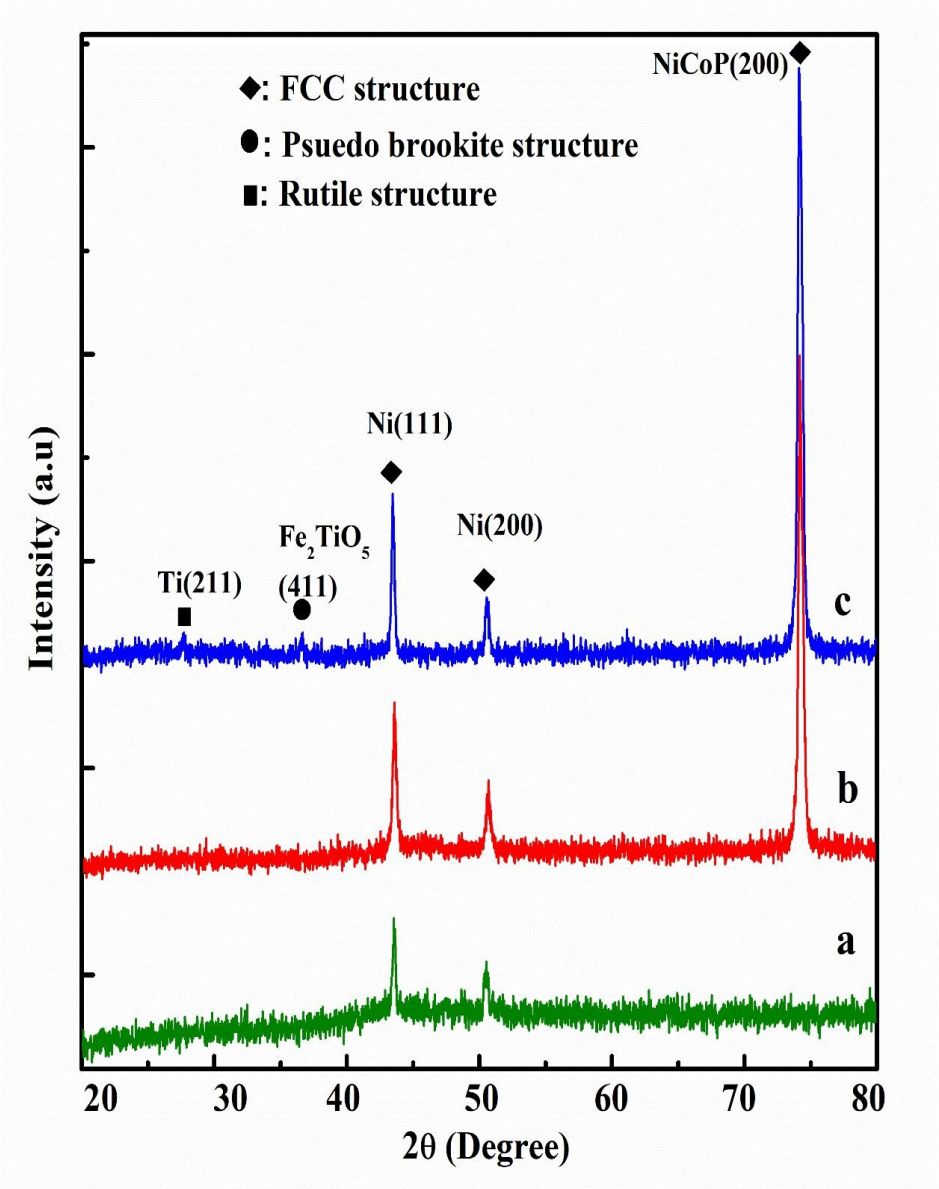

Fig.7. XRD pattern of (a) Ni-P (b) Ni-Co-P (c) Ni-Co-P/FTG coatings over the substrate.

Published on 10 July 2020. Downloaded by Karolinska Institutet University Library on 7/10/2020 4:06:52 PM.

New Journal of Chemistry Accepted Manuscript

View Article Online
DOI: 10.1039/D0NJ00581A

Published on 10 July 2020. Downloaded by Karolinska Institutet University Library on 7/10/2020 4:06:52 PM.

3.8. Evaluation of Electrochemical Activity.

Electrochemical Impedance Spectroscopic (EIS) studies were performed to examine the electrochemical reaction kinetics for a better understanding of the electron transfer process during HER reactions. For the purpose of hydrogen evolution, the metal electrode should contain faradaic resistance, R_F, double layer capacitance, C_{dl} (for some cases C_{dl} is substitute by CPE) and solution resistance, R_s. The HER models varies according to the morphology of electrode (solid, rough and porous) as CPE model where R_s is connected series with the parallel connection of Z_f and C_{dl}, two CPE model where R_s is series with two CPE-R circuit elements and porous electrode model.

An enhanced surface roughness leads to improved catalytic activity by increasing the availability of active surface site for the reaction. The composite incorporated plate has a mixed oxide enriched substrate surface which leads to surface roughness. The change in surface roughness by FTG incorporation was confirmed by R_f (roughness factor) value, which is obtained by taking the ratio of C_{dl} of sample and C_{dl} of smooth metal electrode [41].

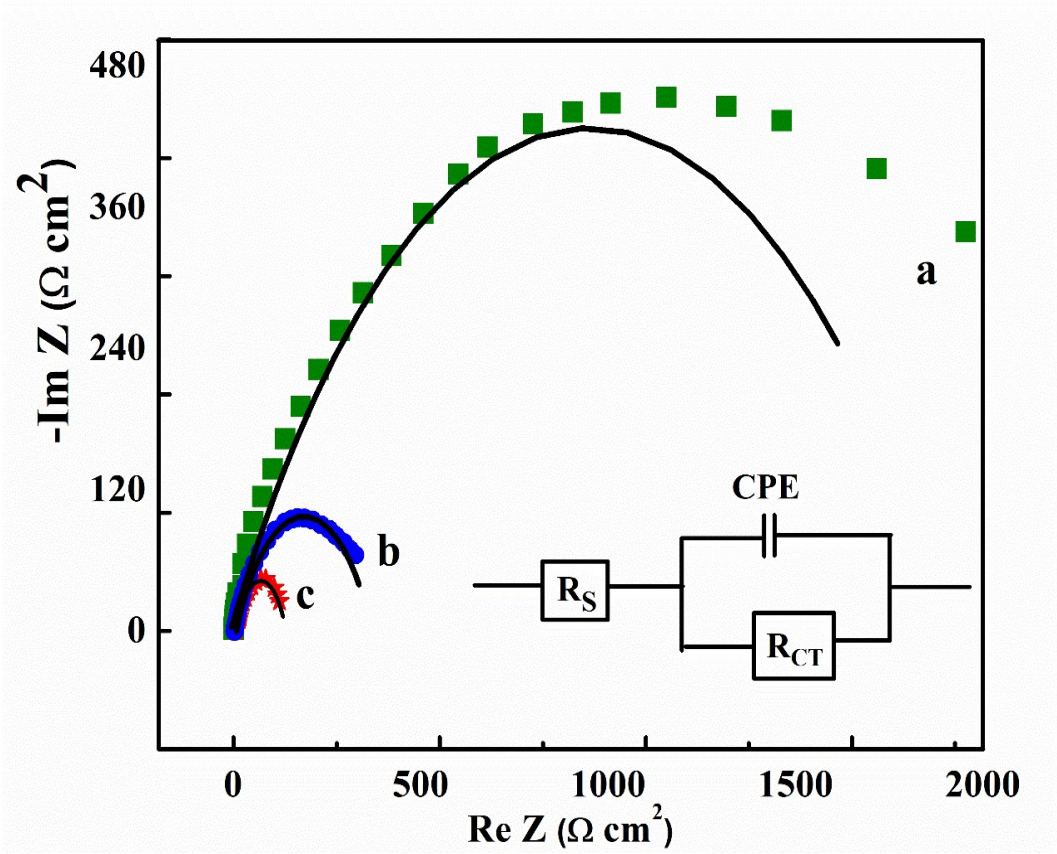

Fig.8. The electrochemical impedance behaviour of electroless coatings (nyquist plot) of (a) Ni-P (b) Ni-Co-P (c) Optimized Ni-Co-P/FTG3 (Insets shows Randles model)

New Journal of Chemistry Accepted Manuscript

View Article Online
DOI: 10.1039/D0NJ00581A

Published on 10 July 2020. Downloaded by Karolinska Institutet University Library on 7/10/2020 4:06:52 PM.

For an ideally polarized electrode, the nyquist plot gives a straight vertical intersecting the Z' axis and the resistance is given by X intersect. But in practical case, there is no such perfectly polarized electrode due to the surface roughness and contamination. Therefore above mentioned straight line is observed intersecting the Z' axis at an angle less than 90 ^{0}C. For most of the cases electrodes with rough and porous surface, the C_{dl} is replaced with CPE in equivalent circuit model. The nyquist plot of Ni-P, Ni-Co-P and Ni-Co-P with FTG coatings are depicted in **Fig.8.** The experimental EIS data in nyquist plot is fitted using the simplified Randles equivalent circuit model which is equivalent to an electrode dipped in electrolyte and the circuit is shown in **inset of Fig.8** and the fitted parameters were depicted in **Table 3.** The model consist of an Ohmic resistance (or solution resistance R_s), double layer capacitance (C_{dl}) and charge transfer resistance (R_{ct}), where C_{dl} is connected parallel with R_{ct} and the whole combination is connected series with R_s [42,43]. In Nyquist plot the intersept at lower frequency (near origin) gives R_s and the intercept at higher frequency (away from origin) gives R_{ct}. Hence the total resistance is the sum of R_s and R_{ct} [44]. Thus the current flow in electrocatalytic interfaces is due to electrochemical reaction (faradaic) and without electrocatalytic reaction (non-faradaic), where the faradaic component arises from R_{ct} or polarization resistance (R_p) and R_s while non-faradaic component arises from C_{dl}. The C_{dl} and R_s is ideal while R_p is non-ideal which contains charge transfer limited activation loss and diffusion limited concentration loss. Both R_{ct} and diffusion resistance occurs at electrode – electrolyte interface and the internal resistance is the sum of R_{ct} and R_p of cathode and anode. A single semicircle nyquist plot was obtained for Ni-P, Ni-Co-P and FTG with coatings, which reveals a controlled charge transfer process during hydrogen evolution. A small distortion as seen in nyquist plot indicates the porous nature of coatings. Since the radius of nyquist semicircle directly point out the charge transfer resistance (R_{ct}), a decrease in R_{ct} value indicate the increased rate of charge transfer process during HER [45]. The FTG incorporated coatings have a small semicircle radius as compared to bare coatings. The increased content over the substrate surface decreases the R_{ct} value due to the increase of surface active sites. The Ni-Co-P/FTG3 was found to have a low R_{ct} value as compare to other FTG incorporated plates due to an increase in active surface site. The presence of FTG contents beyond the optimum concentration of 3 g/L in bath deactivate the surface by inserting strain in lattice catalytic surface and hence show a higher R_{ct} value. Thus its evidence that the composite coating decreases the R_{ct} and hence increases the electrocatalytic activity of modified electrode which is in good consistence with the literature [46-49]. A

New Journal of Chemistry Accepted Manuscript

View Article Online
DOI: 10.1039/D0NJ00581A

comparision between EIS measurements of various HER electrocatalysts were tabulated in **Table.4.**

Fig.9. represent the bode modulus and phase angle plots of coatings in 1 M NaOH solution and the electrode was cathodicaly polarized at a potential of 100 mV, were the rate of HER was measurable. The phase angle, θ_{max} shifted to lower values and the Impedance, |Z| value declined after FTG3 incorporated Ni-Co-P elucidates the enhanced hydrogen evolution rate over the coated surface. The bode phase angle plot only shows sigmoidal peaks without any shoulder illustrate that the proposed Randles circuit have only one double layer capacitance, C_{dl}.

A high value of double layer capacitance (C_{dl}) was observed for composite coatings than bare coatings. The optimized Ni-Co-P/FTG3 plate possesses highest C_{dl} value. A high C_{dl} value ensures enhanced resultant active surface area of composite incorporated plate by increasing the number of catalytic active surface sites. The total charge transfer resistance, R_{ct} was found to be decreases from 1925 Ω to 131.3 Ω indicating superficial activity and enhanced current density of the Ni-Co-P/FTG3 compared to Ni-P and Ni-Co-P for HER.

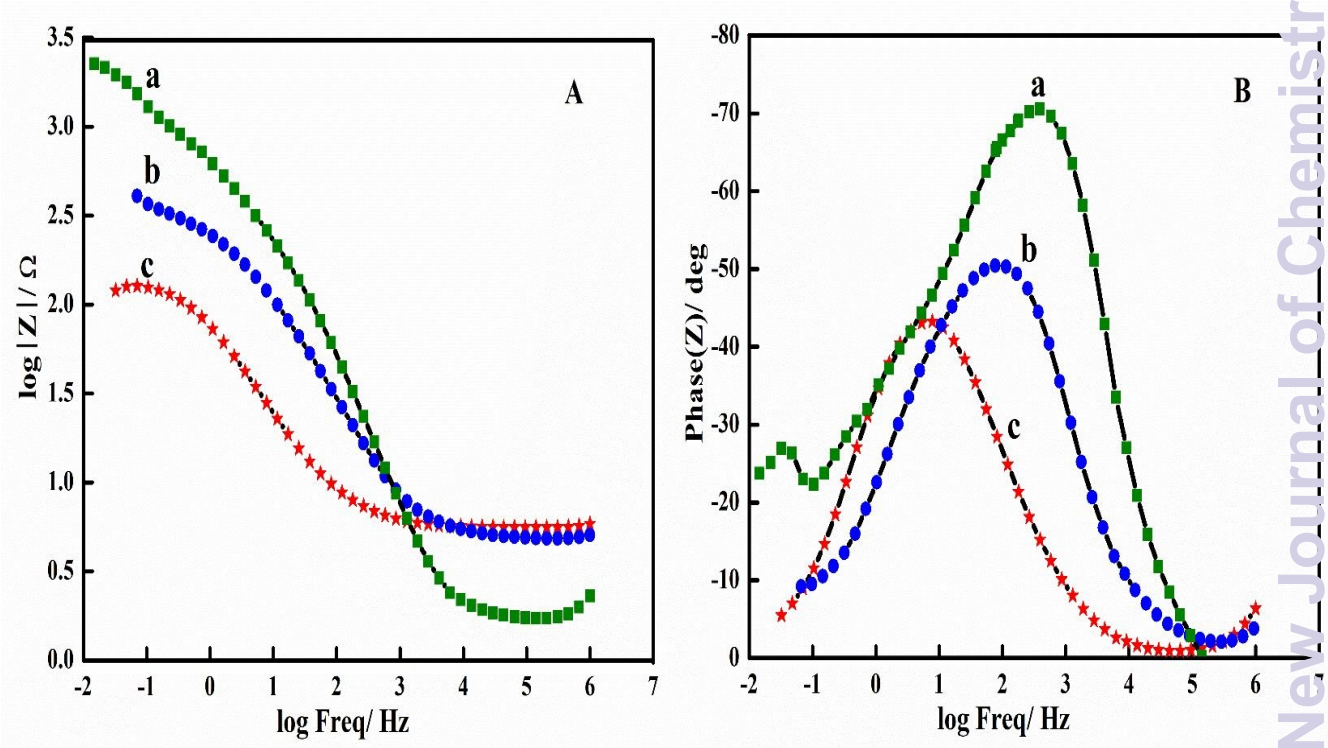

Fig.9. EIS plots (A) Bode modulus and (B) Bode phase angle plots of (a) Ni-P coating (b) Ni-Co-P coating and (c) Ni-Co-P/FTG3 coatings in 1 M NaOH solution at 298 K

Published on 10 July 2020. Downloaded by Karolinska Institutet University Library on 7/10/2020 4:06:52 PM.

New Journal of Chemistry Accepted Manuscript

View Article Online
DOI: 10.1039/D0NJ00581A

Table 3. The electrochemical impedance parameter obtained for various electroless coatings.

Electroless Coatings	R_s (Ω)	C_{dl}	R_{ct} (Ω)	CPE	R_f
Ni-P	-8.91	3.84×10^{-4}	1925	0.442×10^{-4}	19.2
Ni-Co-P	3.95	2.30×10^{-4}	361	0.570×10^{-4}	11.5
Ni-Co-P/FTG3	5.93	15.75×10^{-4}	131.3	2.466×10^{-4}	78.75

Table.4. Comparison of EIS measurements of various HER electrocatalyst

Electrode	R_{ct} (Ω)	C_{dl} (F)	R_f	Reference
IrO_2-Fe_2O_3	232.7	1.38×10^{-3}	69	[46]
IrO_2	693.2	3.05×10^{-3}	152.5	[46]
$MoS_2Se_{2(1-x)}$	85	5.99×10^{-3}	299.5	[47]
Ni-P/IrO_2-TiO_2	540	4.14×10^{-3}	207	[48]
Ni-P/MnO_2-TiO_2	315	1.29×10^{-3}	64.5	[49]
Ni-Co-P/Fe_2O_3- TiO_2-GO	131.3	15.75×10^{-4}	78.75	Present work

A detailed kinetics studies and electrochemical behaviour of coatings was evaluated from tafel parameters obtained from tafel polarization curves derived from the overpotential domain of the Bulter-Volmer equation, which is in the form

$$i = i_0 \left[e^{\left(\frac{(1-\alpha)\eta n F}{RT}\right)} - e^{\left(\frac{-\alpha \eta n F}{RT}\right)} \right] \qquad (11)$$

Where 'R' is the gas constant, 8.314 $JK^{-1}mol^{-1}$ and 'T' is the absolute temperature in kelvin, 'α' in the transfer coefficient or symmetry factor. The catalytic activity of Ni-P, Ni Co-P, Ni-Co-P with varying composition of FTG were explained by the Tafel polarization curves collates in **Fig.10.A**

The alkaline HER mechanism mainly involves three steps as follows [50]:

Published on 10 July 2020. Downloaded by Karolinska Institutet University Library on 7/10/2020 4:06:52 PM.

New Journal of Chemistry Accepted Manuscript

View Article Online
DOI: 10.1039/D0NJ00581A

1. Volmer reaction – Hydrogen adsorption step; $b = \frac{2.3\ RT}{\propto F} \approx 120\ mV$ (12)

2. Heyrovsky reaction – Hydrogen desorption step: $b = \frac{2.3\ RT}{(1-\propto)F} \approx 40\ mV$ (13)

3. Tafel reaction – Recombination of adsorbed hydrogen: $b = \frac{2.3\ RT}{2F} \approx 30\ mV$ (14)

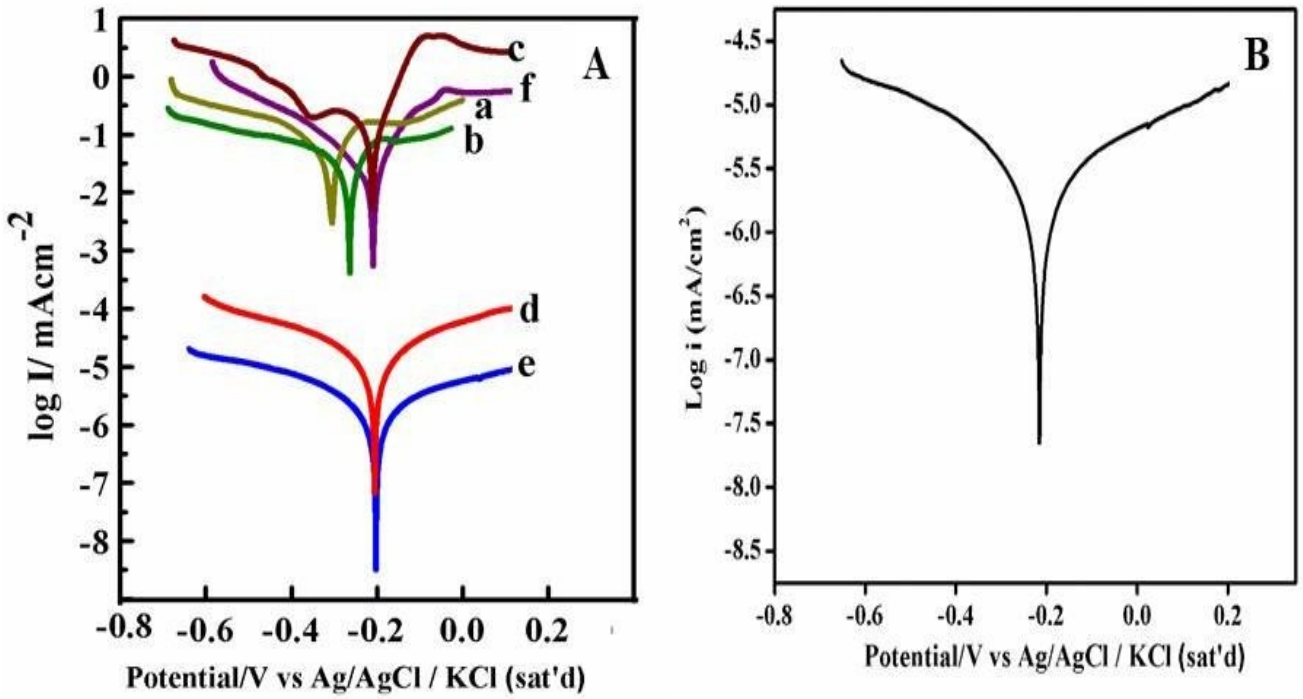

Fig.10. (**A**) Tafel polarization curve of electroless coatings of (a) Ni-P (b) Ni-Co-P (c) Ni-Co-P/FTG1 (d) Ni-Co-P/FTG2 (e) Ni-Co-P/FTG3 and (f) Ni-Co-P/FTG5 and (**B**) Tafel polarization curve of Ni-Co-P/FTG3 coating after HER for 48 hours

Thus hydrogen evolution takes place either by Volmer-Heyrovsky route or by Volmer-Tafel route. The Tafel slope offers an idea about the rate determining steps involving in the reaction. The exchange current density, i_0 corresponds to Ni-P, Ni-Co-P, Ni-Co-P/FTG1, Ni-Co-P/FTG2, Ni-Co-P/FTG3 and Ni-Co-P/FTG5 are 1.34, 1.77, 1.07, 5.11, 6.02 and 2.25 $mAcm^{-2}$ respectively and corresponding overpotential (η) values are 497, 281, 195, 145, 104 and 202 $mVdec^{-1}$, respectively. The FTG incorporation to Ni-Co-P matrix reduces the overpotential value and increases the exchange current density. Among the varying concentration of FTG coatings, the lowest overpotential value was 104 $mVdec^{-1}$ obtained for optimized coating at 10 $mVsec^{-1}$ current density confirms its high efficiency during alkaline HER. A high value of exchange current density of 6.02 $mAcm^{-2}$ for optimized Ni-Co-P/FTG3 coatings unveils its higher electron transfer rate and catalytic activity than other FTG incorporated and bare coatings via the redox system of TiO_2; $TiO_2 \leftrightarrow Ti_2O_3 \leftrightarrow 2TiOOH$ [51]

Published on 10 July 2020. Downloaded by Kaohsiung Institute of University Library on 7/10/2020 4:06:52 PM.

New Journal of Chemistry Accepted Manuscript

View Article Online
DOI: 10.1039/D0NJ00581A

Published on 10 July 2020. Downloaded by Karolinska Institutet University Library on 7/10/2020 4:06:52 PM.

The Tafel slope plot of pure Ni-P, Ni-Co-P and all FTG composite coatings were depicted in **Fig 11.A.** The Tafel slope semi – quantitatively predicts how much faster the reaction occurs at the electrocatalytic interface. From Equation (12) and (13), we can find that the tafel slope (b) is inversely related to charge transfer coefficient (α). Thus for a high value of α, the b value should be small. On the view of HER, b value often predicts the reaction mechanism at catalytic interface. For a low value of b about 30 mv/dec and 40 mv/dec corresponds to Tafel and Heyrovsky reaction mechanism, respectively whereas a high value of b of about 120 mv/dec corresponds to Volmer reaction mechanism as shown in equation (12) – (13). In order to reduce overpotential or activation energy in electrode interface we should have also consider the electrocatalytic surface configuration and electrode material. If the rate determining step (RDS) is Volmer, indicates the electrode material with a high degree of cavities and surface edges while if the RDS is Heyrovsky or Tafel which reveals the electrocatalytic material with high surface roughness which in turn increases the surface area and rate of electrolysis. Tafel slopes of Ni-P, Ni-Co-P, Ni-Co-P/FTG1, Ni-Co-P/FTG2, Ni-Co-P/FTG3 and Ni-Co-P/FTG5 was found to be 118, 109, 42, 39, 37 and 44 $mVdec^{-1}$. The FTG3 coated Ni-Co-P has a least slope of 37 mV/dec^{-1} as compared to all other coated plates, which is in good agreement with literature [50] that the optimized composite incorporation in Ni-P coating cause a shift in the value of Tafel slope. Thus the Tafel slope value indicates that there is a possible change in HER mechanism pathway from Volmer in case of pure Ni-P coating to Heyrovsky in case of Ni-Co-P/FTG. So the hydrogen evolution mechanism was proposed to be Volmer-Heyrovsky.

The stability of FTG coating was confirmed by analysing the tafel parameters of FTG incorporated Ni-Co-P coatings after HER as shown in **Fig.10.B.** The data shows that there were no considerable changes in overpotential (η) and tafel slopes for composite coating after HER. All these factors account for the extra stability attained by Ni-P plates after reinforcement and incorporation of Co and FTG composite into Ni-P matrix.

The LSV plots for Ni-P, Ni-Co-P and composite coatings were depicted in **Fig.11.B.** The potential in standard calomel electrode can be converted into RHE by following equation

$$E_{RHE} = E_{SCE} + 1.068\ V \qquad (15)$$

The curve shows a high onset potential value for Ni-P coating and a lowest onset potential for optimized FTG coated plate. Thus FTG3 incorporated plate shows high HER activity than all other electrodes. The enhanced catalytic activity of Co incorporated plates

New Journal of Chemistry Accepted Manuscript

View Article Online
DOI: 10.1039/D0NJ00581A

was confirmed by the low shift in onset potential of Ni-Co-P than pure Ni-P, due to the increasing number of negatively charged active sites of phosphorous for H^+ adsorption [52].

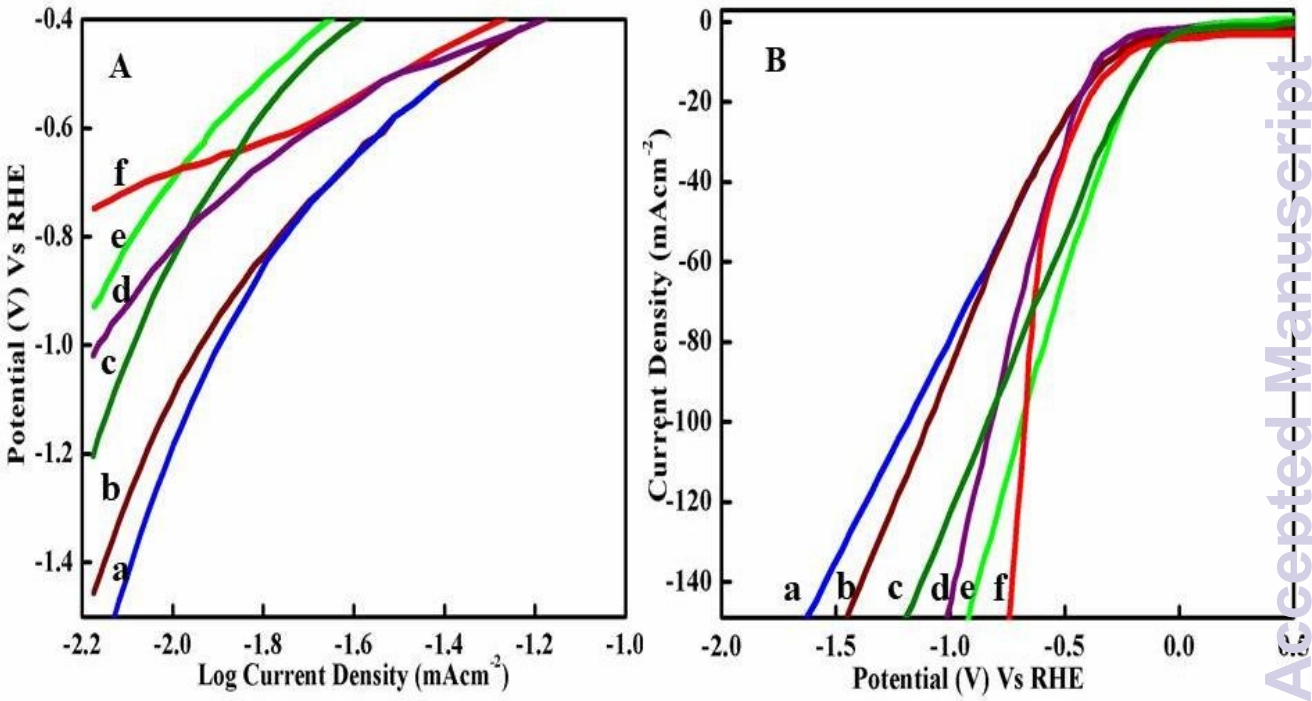

Fig.11. Tafel slope plot (**A**) and LSV curve (**B**) of (a) Ni-P (b) Ni-Co-P (c) Ni-Co-P/FTG1 (d) Ni-Co-P/FTG2 (e) Ni-Co-P/FTG5 and (f) Ni-Co-P/FTG3

3.9. Hydrogen adsorption during HER process

A potentiostatic technique was carried out in 1 M NaOH, the electrode was cathodically polarizes at -1.23 V, which is attributed to the hydrogen adsorption over the catalytic surface. At -0.65 V the adsorbed hydrogen is reversibly oxidized from the electrode and the extent of hydrogen adsorption was evaluated from the area under the current density versus time curve as shown in **Fig.12.A.** The coatings with optimized FTG content (FTG3) have a large area under the current density-time curve and hence it possess a higher extent of H adsorption than all other coated plates [48]. The charge value of optimized plates was found to be higher than Ni-P and Ni-Co-P coated plate. Based on these electrochemical data, the optimized composite coating (FTG3) over substrate enhance the cathodic property of the electrode as well as stability.

Published on 10 July 2020. Downloaded by Karolinska Institutet University Library on 7/10/2020 4:06:52 PM.

New Journal of Chemistry Accepted Manuscript

View Article Online
DOI: 10.1039/D0NJ00581A

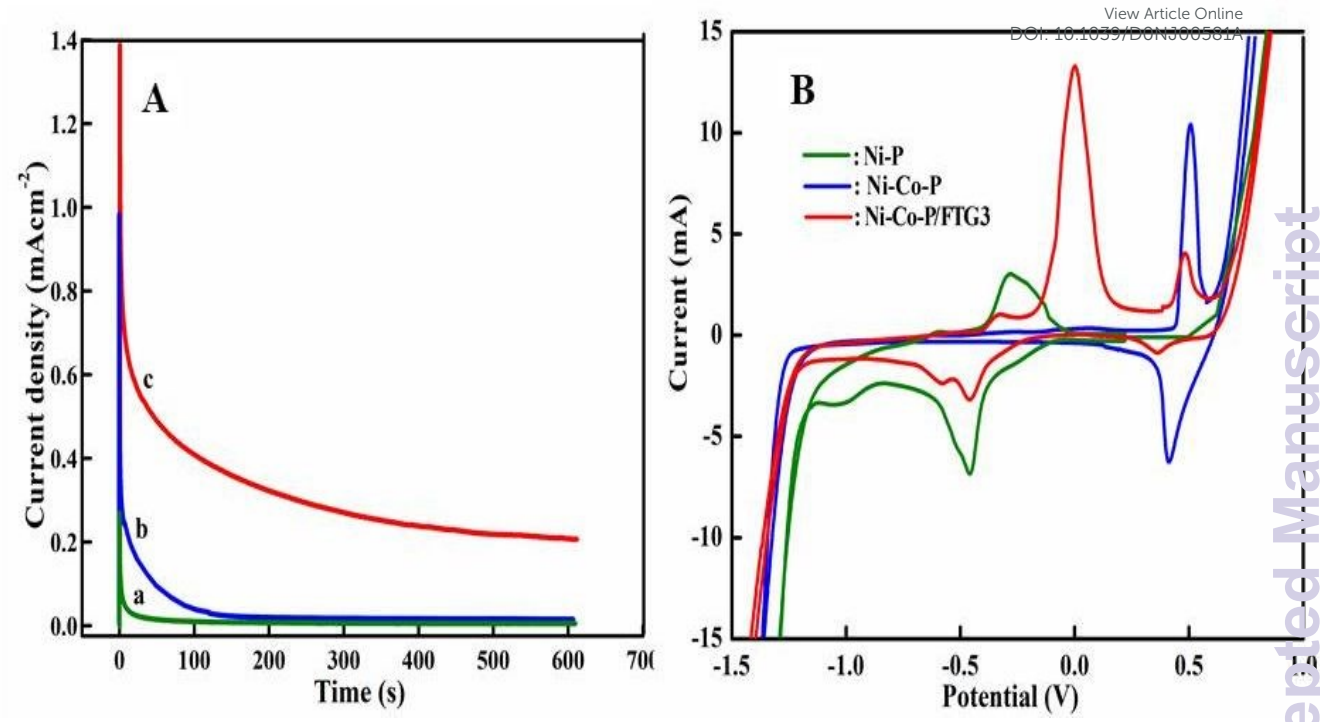

Fig.12. (**A**) Potentiostatic curve of (a) Ni-P (b) Ni-Co-P (c) Ni-Co-P/FTG3 (**B**) Cyclic voltammogram of various coatings over Cu substrate in 0.1 M NaOH solution

The redox characteristics of electroless Ni-P, Ni-Co-P and various concentration of FTG coatings were investigated by cyclic voltametric analysis in 0.1 M NaOH solution at a scan rate of 100 mV/s which is depicted in **Fig.12.B.** The figure illustrated that the Ni-P and Ni-Co-P coatings exhibit a redox peak at low current whereas FTG composite incorporated coatings exhibit redox peak at high current values. This authenticates its potential electrocatalytic nature, which may be due to the increase in surface area and synergic effects arise within the composite and Ni-Co-P on electrode surface which attributes an enhanced conduction route for electron transfer kinetics.

3.10. Polarization Studies of Coatings

In order to carry out the polarization studies of electroless coatings, cathodic polarization curves for pure Ni-P was compared with Ni-Co-P and varying concentration of FTG incorporated Ni-Co-P coatings and depicted in **Fig.13.A.** The polarization curve shows that the electroless plate obtained by 3 g/L FTG composite in plating bath shows a low shift to negative potential region as compared to the pure Ni-P, pure Ni-Co-P and other FTG incorporated Ni-Co-P plates. The polarization studies reveals that the cobalt deposition and FTG incorporation onto Ni-P surface leads to an effective charge separation and electron transfer from the substrate surface. As the result of this increased electron transfer process, the

Published on 10 July 2020. Downloaded by Karolinska Institutet University Library on 7/10/2020 4:06:52 PM.

New Journal of Chemistry Accepted Manuscript

View Article Online
DOI: 10.1039/D0NJ00581A

rate of HER increases with lower overpotential. If the FTG concentration increases beyond the optimum concentration level, which dramatically reduces the charged species over the substrate surface due to the back-bonding, as a result of the charge delocalization the catalytic activity for HER is lower.

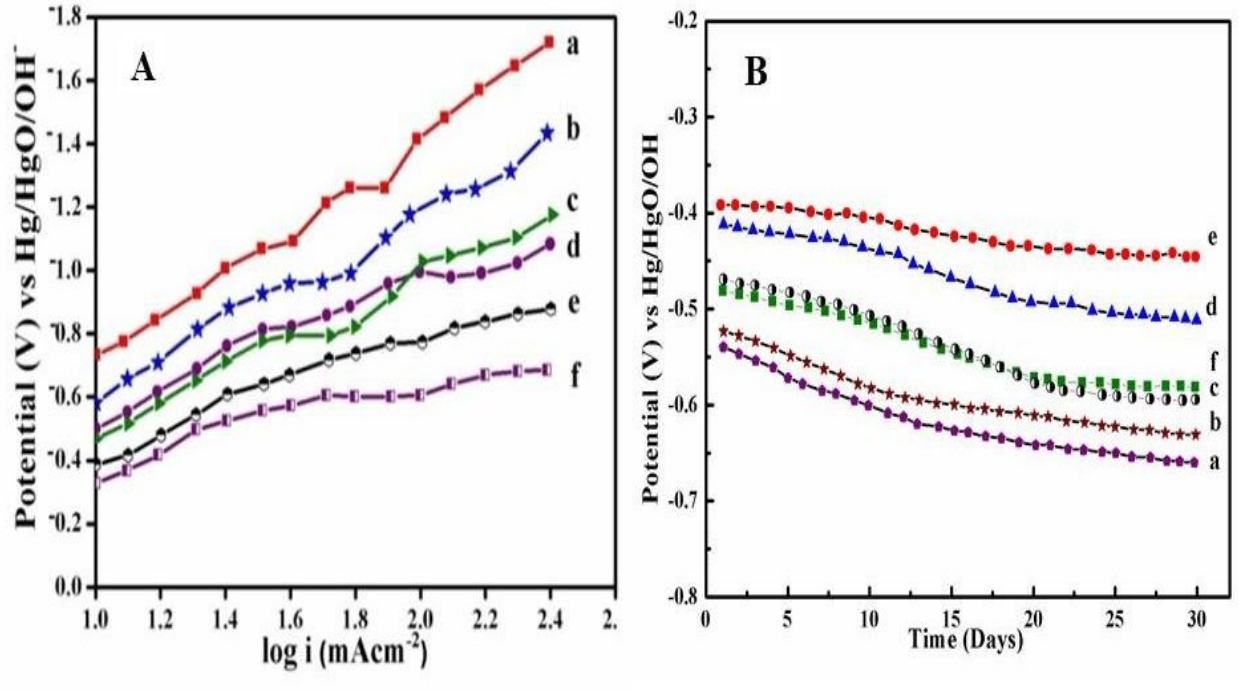

Fig.13. (**A**) Cathodic polarization curves for coatings of (a) pure Ni-P (b) Ni-Co-P (c) Ni-Co-P/ FTG1 (d) Ni-Co-P/ FTG 5 (e) Ni-Co-P/ FTG2 (f) Ni-Co-P/FTG3 and (**B**) OCP analysis of (a) Ni-P (b) Ni-Co-P (c) Ni-Co-P/FTG1 (d) Ni-Co-P/FTG2 (e) Ni-Co-P/FTG3 and (f) Ni-Co-P/FTG5

The long term stability of FTG incorporated Ni-Co-P plates towards HER activity was carried out by open circuit potential analysis in 1 M NaOH solution for 30 days. The data in the **Fig.13.B** reveals that the optimized FTG incorporated plate (FTG3) shows a lower potential response (-0.39 to -0.42 V), whereas all other coated plates exhibit a higher cathodic potential shift. This ensures the enhanced stability and durability of Ni-Co-P/FTG3 plate.

3.11. Electrochemical performance

The electrocatalytic performance of prepared samples were assessed with the catalysts already reported in literature which was illustrated in **Table 5**. The catalytic performances are superior to these of the state-of-the-art Fe-Ni based catalysts reported so far.

Published on 10 July 2020. Downloaded by Karolinska Institutet University Library on 7/10/2020 4:06:52 PM.

New Journal of Chemistry Accepted Manuscript

View Article Online
DOI: 10.1039/D0NJ00581A

Table 5. Comparison of electrochemical parameters of various TiO_2 based electrodes for electrocatalytic hydrogen evolution

Electrode	Medium	η(mV)	b (mV/dec)	Reference
IrO_2/TiO_2	0.5 M H_2SO_4	-107	46.8	[53]
CoS_2/TiO_2	1 M KOH	-198	55	[54]
Co_9S_8/TiO_2	1 M KOH	-150	71	[55]
$Cu\text{-}Cu_2O/TiO_2$	1 M KOH	-114	67	[56]
$Ni\text{-}P/TiO_2$	0.5 M H_2SO_4	-209	46.6	[57]
Ni_xCo_yP /TiO_2	0.5 M H_2SO_4	-100	120	[57]
$WS_2\text{-}TiO_2$	1 M KOH	-142	120	[58]
$Ni\text{-}P/TiO_2\text{-}MnO_2$	32 % NaOH	-142	68.9	[49]
$Pt\text{-}Mo_2C/TiO_2$	0.5 M H_2SO_4	-67	39.3	[59]
TiO_2/Ni_3S_2	1 M KOH	-112	69	[60]
$C/NiO/TiO_2$	Nickel acetate	-86	67.1	[61]
MoS_2/TiO_2	0.5 M H_2SO_4	-640	100	[62]
TiO_2NB/TiO_2NS -Au	0.5 M H_2SO_4	-510	58	[63]
TiO_2NB/TiO_2NB -Au	0.5 M H_2SO_4	-450	51.4	[63]
$TiO_2/RuO_2\text{-}Mn$	0.1 M H_2SO_4	-386	50	[64]
TiO_2 NW/MoS_2	0.5 M H_2SO_4	-350	48	[65]
TiO_2 NW/MoS_2	1 M KOH	-700	60	[65]
$Au/TiO_2/Pd$	0.1 M H_2SO_4	-210	231	[66]
$NiCoP/Fe_2O_3\text{-}TiO_2\text{-}GO$	1 M NaOH	-104	37	The present work

All these factors collaboratively illustrates the outstanding electrocatalytic performance Ni-Co-P/FTG3 over materials reported in literature [53-66] though as-synthesised materials still show lower activity than that of Pt/C. The enhanced catalytic activity of Ni-Co-P/FTG3 catalysts was ascribed the surface activity enrichment due to GO exfoliation and synergistic effect of elements associated with the coated composite.

4. Summary

In summary, we have successfully synthesize cathodic electrode coated with Ni-Co-P via electroless route and it is modified with FTG matrix, its high performance electrocatalytic

Published on 10 July 2020. Downloaded by Karolinska Institutet University Library on 7/10/2020 4:06:52 PM.

New Journal of Chemistry Accepted Manuscript

View Article Online
DOI: 10.1039/D0NJ00581A

activity towards HERs in alkaline media was studied. Thermal decomposition method induces the structural evolution of catalysts from its precursors, which leads to well-tuned electrocatalysts. The incorporation of Co to binary Ni-P alloy increase its HER activity of electrode due to synergic effect of elements in Ni-Co-P and transfer of electron density from Co or Ni to P creating electroactive centres for HER. The HER kinetics follows through Volmer-Heyrovsky mechanism with a low value of overpotential and Tafel slope. FTG coating on to catalytic surface plays a vital role in inducing surface roughness, porosity and increased active sites which confirmed from high C_{dl} and low R_{ct} values. The FTG incorporated electrode was better choice as a cathode material for HER. Therefore this study envisages a new strategy for the design of economically benign catalysts towards HERs.

Conflicts of interest

The authors declare that they have no competing interests.

Acknowledgements

The authors are thankful to Principal, Sree Narayana College, Kollam, Kerala, India and Professor and Head, Department of Chemistry, Sree Narayana College, Kollam, Kerala, India for providing the laboratory facilities. One of the authors, Sarika. S is grateful to University of Kerala, Trivandrum, Kerala, India, for providing assistance in the form of research fellowship for carried out this work.

REFERENCES

1 M.Zhang, N.Xu, G.Cao, Z. Chen, J. Cui, L.Gan, H. Dai, X. Yang, P. Wang. ACS Cat. 2018, 8, 5062-5069.,

2 J. Zhang, T. Wang, P. Liu, Z. Liac, S. Liu, X. Zhuang, M. Chen, E. Zschech, X. Feng. Nat. Commun., 2017,8, 15437

3 M. Zeng , Y. Li. J. Mater. Chem. A., 2015, 3, 14942–14962.

4 J. Yan, Y. Zhang, Y. Huang, Y. E. Miao, T. Liu. Adv. Mater. Interfaces., 2017, 4, 1–7.

5 H. Yin, s. zhao, K. Zhao, A. Muqsit, H. Tang, L. Chang, Z. Nat. Commun., 2015, 6, 1–8.

6 B. Pal, T. Hata, K. Goto, G. Nogami. J. Mol. Catal. A Chem., 2001, 169, 147–155.

7 R. Q. Long, R. T. Yang. J. Catal., 2002, 207, 158–165.

Published on 10 July 2020. Downloaded by Karolinska Institutet University Library on 7/10/2020 4:06:52 PM.

New Journal of Chemistry Accepted Manuscript

View Article Online
DOI: 10.1039/D0NJ00581A

Published on 10 July 2020. Downloaded by Karolinska Institutet University Library on 7/10/2020 4:06:52 PM.

8 K. E. Dekrafft, C. Wang, W. Lin. Adv. Mater., 2012, 24, 2014–2018.

9 A. Khaleel. Colloids Surf. A Physicochem. Eng. Asp. 2009, 346, 130–137.

10 M. M. Jakšić. Int. J. Hydrog. Energy., 1987, 12, 727–752.

11 B. Łosiewicz, A. Budniok, E. Rówiński, E. Łagiewka, A. Lasia. Int. J. Hydrogen Energy., 2004, 29, 145–157.

12 H. Li, Z. Sui. New. J. Chem., 2019, 43, 17963-17973.

13 W. S. Hummers, R. E. Offeman. J. Am. Chem. Soc., 1958, 80, 1339.

14 H. Jin, S. Jiang, L. Zhang. J. Rare Ear., 2009, 27, 109-113.

15 T. Burchardt. Int. J. of Hydrog. Ener.,2002, 27, 323-328

16 D. Chinnadurai, P. Karuppian, S. M. Chen, H. J. Kim, K. Prabakar. New J. Chem., 2019, 43, 11653-11659.

17 Y. Cao, W. Yang, W. Zhang, G. Liu, P. Yeu. New J. Chem., 2004, 28, 218–222.

18 G. Shirane, S. J. Pickart, R. Nathans, Y. Ishikawa, J. Phys. Chem. Solids., 1959, 10, 35-43.

19 F.C. Gennari, J. J. Andrade Gamboa, D.M. Pasquevich, J. Mater. Sci. Lett. 1998, 17, 687-689.

20 J. A. Wang, R. Limas-Ballesteros, T. Lopez, A. Moreno, R. Gomez, O. Novaro, and X. Bokhimi. J. Phys.Chem. B., 2001, 105(40), 9692-9698.

21 D. S. Ginley, M. A. Butler. J. Appl. Phys., 1977, 48, 2019–2021.

22 B. Pal, M. Sharon, G. Nogami. Mater. Chem. Phys., 1999, 59, 254-261.

23 R. Suresh, K.Giribabu, M. Manigandan, A. Stephen, V. Narayanan. RCS Adv., 2014, 4, 17146-17155.

24 T.Somanathan, K. Prasad, K. Ostrikov, A. Saravanan, V. M. Krishna. Nanomaterials., 2015, 5, 826-834.

25 N. R. Wilson, P.A. Pandey, R. Beanland, R.J. Young, L.A. Kinloch, L. Gong, Z. Liu, K. Sunega, J. P. Rourke, S. J. York, J. Sloan. ACS Nano., 2009, 3, 2547-2556.

New Journal of Chemistry Accepted Manuscript

View Article Online
DOI: 10.1039/D0NJ00581A

Published on 10 July 2020. Downloaded by Karolinska Institutet University Library on 7/10/2020 4:06:52 PM.

26 A. P. Grosvenor, B. A. Kobe, M. C. Biesinger, N. S. McIntyre. Surf. Interface Anal., 2004, 36, 1564-1574.

27 B. Sun, T. Shi, Z. Peng, W. Sheng, T. Jiang, G. Liao. Nanoscale Res. Lett., 2013, 8, 1-8.

28 F. T. Johra, W. G. Jung. Appl. Surf. Sci., 2015, 357, 1911-1914.

29 J. N. Balaraju, S. N. Sankara narayanan, S. K. Sh. J. Appl. Electrochem., 2003, 33, 807–816.

30 E. M. Fayyad, A. M. Abdullah, M. K. Hassan, A. M. Mohamed, G. Jarjoura, Z. Farhat. Emergent Mater., 2018, 1, 3-24.

31 A. Grosjean, M. Rezrazi, P. Berçot. Surf. Coatings Technol., 2000, 130, 252-256.

32 H. Ashassi-Sorkhabi, A. Mirmohseni, H. Harrafi. Electrochim. Acta., 2005, 50, 5526–5532.

33 J. N. Balaraju, T. S. N. Sankara Narayanan, S. K. Seshadri. Mater. Res. Bull., 2006, 41, 847-860.

34 F. Hou, W. Wary, H. Guo. Appl. Surf. Sci., 2006, 252, 3812-3817.

35 W. Chen, W. Gao, Y. He. Surf. Coatings Technol., 2010, 204, 2493-2498.

36 L. T. Shi, J. Hu, L. Fang, F. Wu, X. L. Liao, F. M. Meng. Mater. Corros., 2016, 67, 1034-1041.

37 D. Seifzadeh, A. R. Hollgh. J. Mater. Eng. Perform., 2014, 23, 4109-4121

38 K. N. Srinivasan, T. Selvaganapathy, R. Meenakshi, S. John. Surf. Eng., 2011, 27, 65-70.

39 Y. Wu, C. C. Wan, Y. Y. Wang. J. Electron. Mater., 2005, 34, 541-550.

40 J. N. Balaraju, T. S. N. Sankara Narayanan, S. K. Seshadri. J. Appl. Electrochem., 2003, 33, 807.

41 L. Birry, A. Lasia. J. Appl. Electrochem., 2004, 34, 735-749.

42 S. Shyamal, P. Hajra, H. Mandal, A. Bera, D. Sariket, A. K. Satpati, S.Kundu, C. Bhattacharya. J. Mater. Chem. A., 2016, 4, 9244-52.

43 B. Klahr, S. Gimenez, F. Fabregat-Santiago, T. Hamann, J. Bisquert. Journal of the

New Journal of Chemistry Accepted Manuscript

View Article Online
DOI: 10.1039/D0NJ00581A

American Chemical Society., 2012,134, 4294-302.

44 N. Sekar, R. P. Ramasamy. J. Microb. Biochem. Technol. S. 2013;6.

45 X.Chen, Z. Pan, C. Lei, Y. Jin, B. Yang, Z. Li, X. Zhang, L.Lei, C. Yuan. J. Mater. Chem. A.,2019, 7, 965-971.

46 X.Yang, Y. Li, L. Deng, W. Li, Z. Ren, M. Yang, X. Yang, Y. Zhu. RSC advances., 2017,7,20252-8.

47 B. Lin, Z. Lin, S. Chen, M. Yu, W. Li, Q. Gao, M. Dong, Q. Shao, S. Wu, T. Ding, Z. Guo. Dalton Transactions., 2019,48,8279-87.

48 S. M. A. Shibli, V. S. Dilimon. J. Solid State Electrochem., 2007, 11, 1119-1126

49 S. M. A. Shibli, M. A. Sha, B. L. Anisha, D. Ponnamma, K. K. Sadasivuni. J. Electroanalytical Chemistry., 2018, 826, 104-116.

50 A. R. Madram, S. Asadi. New. J. Chem., 2017, 41, 3344-3351

51 D. Gierlotka, E. Rovinski, A. Budnoik, E. Lagiewka. J. Appl. Electrochem., 1997, 27,1349.

52 P. Jiang, Q. Liu, X. Sun. Nanoscale., 2014, 6, 13440-13445.

53 M. Yuan, Y. Zhu, L. Deng, R. Ming, A. Zhang, W. Li, B. Chai, Z. Ren. New J. Chem., 2017,41, 6152-6159.

54 P. Ganesan, A. Sivanantham, S. Shanmugam. J. Mater. Chem. A., 2018, 6, 1075–1085.

55 F. Yang, S. Deng, S. Lin, M. Chen, X. Xia, X. Lu. Nanotechnology., 2019, 30, 404001.

56 B. Long, H. Yang, M. Li, M. S. Balogun, W. Mai, G. Ouyang, Y. Tong, P. Tsiakaras, S. Song. Appl. Catalysis B: Environmental., 2019, 243, 365-72.

57 Y. Li, P. Yang, B. Wang, Z. Liu. Beilstein J. Nanotechnology., 2019, 10, 62-70.

58 S. Liu, Y. Xu, D. Chanda, L. Tan, R. Xing, X. Li, L. Maoa, N. Kazuyab, A. Fujishima. International J. of Hydrogen Energy., 2020, 45, 1697-1705.

59 Y. Liu, L. Wan, J. Wang, L. Cheng L, R. Chen R, Ni H. Applied Surface Science., 2020, 509, 144679.

Published on 10 July 2020. Downloaded by Karolinska Institutet University Library on 7/10/2020 4:06:52 PM.

New Journal of Chemistry Accepted Manuscript

View Article Online
DOI: 10.1039/D0NJ00581A

60 S. Deng, K. Zhang, D. Xie, Y. Zhang, Y. Zhang, Y. Wang, J. Wu, X. Wang, H. J. Fan, X. Xia, J. Tu. J. Nano-Micro Letters., 2019, 11.

61 J. Yang, L. Cheng, L. Wan, J. Yan, R. Chen, H. Ni. Electrochemistry Communications., 2018, 97, 68-72.

62 A. Pal, S. Dutta, T. K. Jana, K. Chatterjee. AIP Conference Proceedings., 2019, 2115, 030165.

63 M. Li, H. Liu, Y. Song, Z. Li. Materials Characterization., 2019, 151, 286-91.

64 M. E. C. Pascuzzi, A. Goryachev, J. P. Hofmann, E. J. Hensen. Applied Catalysis B: Environmental., 2020, 261, 118225.

65 A. Tahira, Z. H. Ibupoto, R. Mazzaro, S. You, V. Morandi, M. M. Natile, M. Vagin, A. Vomiero. ACS Applied Energy Materials., 2019, 2, 2053-2062.

66 K. M. Emran. Int. J. Electrochem.Sci., 2020, 15, 4218-4231.

Published on 10 July 2020. Downloaded by Karolinska Institutet University Library on 7/10/2020 4:06:52 PM.

New Journal of Chemistry Accepted Manuscript

View Article Online
DOI: 10.1039/D0NJ00581A

Graphical Abstract

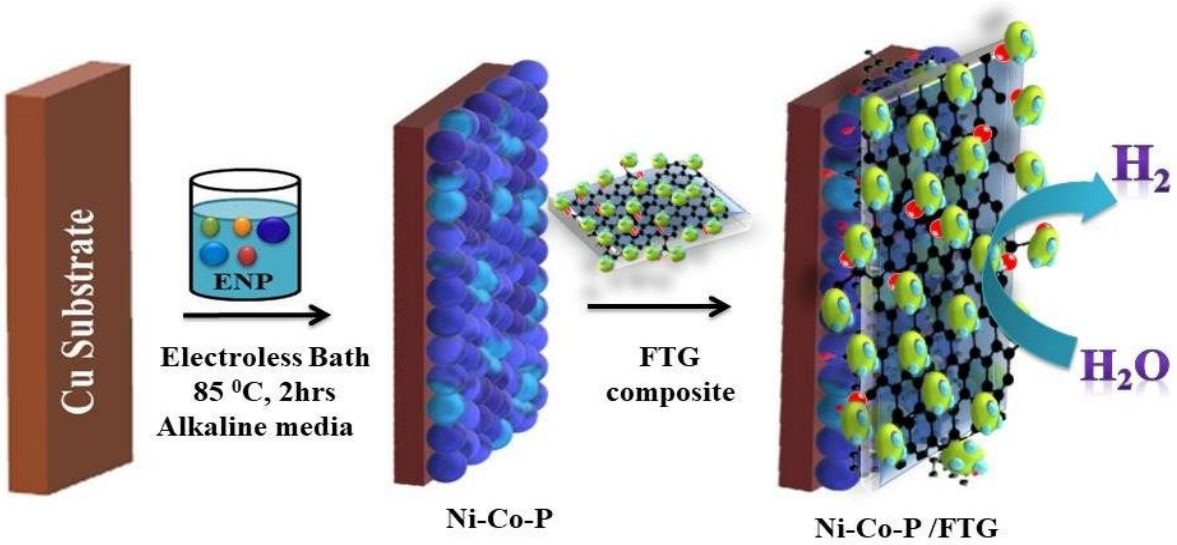

Published on 10 July 2020. Downloaded by Karolinska Institutet University Library on 7/10/2020 4:06:52 PM.

New Journal of Chemistry Accepted Manuscript